THE GEOLOGICAL SOCIETY OF AMERICA®

Oceanic plateau subduction during closure of the Bangong-Nujiang Tethyan Ocean: Insights from central Tibetan volcanic rocks

Lu-Lu Hao[1,2], Qiang Wang[1,2,3,†], Chunfu Zhang[4], Quan Ou[1,2], Jin-Hui Yang[5], Wei Dan[1,3], and Zi-Qi Jiang[6]

[1]*State Key Laboratory of Isotope Geochemistry, Guangzhou Institute of Geochemistry, Chinese Academy of Sciences, Guangzhou 510640, China*

[2]*University of Chinese Academy of Sciences, Beijing 10069, China*

[3]*Chinese Academy of Science Center for Excellence in Tibetan Plateau Earth Sciences, Beijing 100101, China*

[4]*Department of Geosciences, Fort Hays State University, Hays, Kansas 67601-4099, USA*

[5]*Institute of Geology and Geophysics, Chinese Academy of Science, Beijing 100029, China*

[6]*School of Earth Science, Guilin University of Technology, Guilin 541004, China*

ABSTRACT

Identification of arc magmatic rock associations in a subduction zone has important implications for specifically revealing the geodynamic evolution of the subduction system. The closure time of the Bangong-Nujiang Tethyan Ocean and the detailed subduction processes have been hotly debated, hindering our understanding of the tectonic evolution of central Tibet. Here, we investigated the ca. 110–104 Ma Gerze lavas (basalts, basaltic andesites, andesites, dacites, and rhyolites) in southern Qiangtang. Fusion of slab fluid-metasomatized mantle wedge could yield the basalts, and such basaltic magmas, if contaminated with ancient basement orthogneisses, could have formed the andesites. The basaltic andesites with high Nb and Nb/La are similar to the Nb-enriched arc basalts and probably originated from slab melt-metasomatized mantle. The dacites were generated by fractional crystallization of the subducted mélange-derived intermediate magmas. The rhyolites have geochemical characteristics (high SiO_2 and La/Yb; low MgO and Sr/Y) similar to those of Jamaican-type adakites and were possibly sourced from the subducted oceanic plateau at low pressures. The Gerze Jamaican-type adakites and Nb-enriched basalt association could imply intense slab-mantle interactions. The Gerze lava suites show clear arc affinities, indicating that oceanic subduction may have lasted until 100 Ma. Based on previous studies and a noticeable ca. 145–125 Ma magmatic lull in southern Qiangtang, we suggest that the Bangong-Nujiang oceanic subduction geodynamics involved normal subduction (170–145 Ma), flat subduction (145–125 Ma), and slab roll-back (125–101 Ma). Moreover, the flat subduction was most likely caused by subduction of the oceanic plateau. Therefore, we propose, for the first time, that Tethyan oceanic plateau subduction during the Early Cretaceous could explain the tectonic evolution of the Bangong-Nujiang Ocean and distinctive magmatism in southern Qiangtang, central Tibet.

INTRODUCTION

Subduction zones are important regions on Earth where substantial crustal materials can be incorporated into the mantle. During this recycling process, intense arc magmatism can occur by partial melting of the subducted slab, the slab fluid- or melt-metasomatized mantle wedge, and the overlying crust (Pearce and Peate, 1995; Castillo et al., 2002). Variable subduction processes can induce distinct magmatic rock associations. For example, A-type granites and intraplate-type basalts are often produced during ridge subduction and slab break-off (Tang et al., 2010). Flat slab subduction and subsequent roll-back induce a magmatic lull and ensuing magmatic flare-up, respectively (Gutscher et al., 2000). These special subduction cases are likely responsible for generation of slab-derived adakites, which can drastically change the magma genesis from typical fluid-related calc-alkaline magmatism in normal arcs to melt-related magmatism (adakite–high-Mg andesite–Nb-enriched basalt; Bourdon et al., 2003). Thus, identification of arc magmatic rock associations in a subduction zone has important implications for specifically revealing the geodynamic evolution of the subduction system.

The Bangong-Nujiang suture zone, representing a remnant of the Bangong-Nujiang Tethyan Ocean, is located in the central Tibetan Plateau and is a significant Tethyan suture that separates the southern Qiangtang block in the north from the Lhasa block in the south (e.g., Yin and Harrison, 2000). The evolution of the Bangong-Nujiang Ocean could strongly constrain the Mesozoic tectonic history of central Tibet, where substantial metallogenesis has recently been reported (Geng et al., 2016). Numerous studies have suggested that Mesozoic magmatism in southern Qiangtang should be attributed to the northward subduction of the Bangong-Nujiang Ocean and ensuing Lhasa-Qiangtang collision (e.g., J.X. Li et al., 2014; Zhang et al., 2012; Y.X. Zhang et al., 2017). However, the timing of closure of the Bangong-Nujiang Ocean remains controversial, and, accordingly, the subduction geodynamics have been hotly debated (e.g., Zhu et al., 2016), greatly hindering our understanding of the tectonic evolution of central Tibet.

Two main closure ages of the Bangong-Nujiang Ocean have been suggested: the late Early Cretaceous (ca. 100 Ma, e.g., Wang et al., 2016; K.J. Zhang et al., 2012, 2014; Y.X. Zhang et al., 2017; Zhu et al., 2006; J.X. Li et al., 2014; Fan et al., 2015) and the Late Jurassic (ca. 160–145 Ma, e.g., Li et al., 2017; Kapp et al., 2007; Zhang, 2004; Zhang et al., 2004; Zhu et al., 2016). For instance, in recent years,

†Corresponding author: State Key Laboratory of Isotope Geochemistry, Guangzhou Institute of Geochemistry, Chinese Academy of Sciences, Guangzhou 510640, China; wqiang@gig.ac.cn.

GSA Bulletin; May/June 2019; v. 131; no. 5/6; p. 864–880; https://doi.org/10.1130/B32045.1; 10 figures; Data Repository item 2018295; published online 29 November 2018.

several exposures of Early Cretaceous oceanic basaltic rocks have been identified within the Bangong-Nujiang suture zone, and the oceanic basalts and related sedimentary rocks have been widely interpreted as parts of ophiolites and may imply that the Bangong-Nujiang Ocean could have survived until the Late Cretaceous (ca. 100 Ma; e.g., Bao et al., 2007; Wang et al., 2016; K.J. Zhang et al., 2012, 2014). This is consistent with broad paleomagnetic investigations across the Bangong-Nujiang suture zone (e.g., Otofuji et al., 2007; Tong et al., 2015; Song et al., 2017). However, Zhu et al. (2016) suggested that these Cretaceous basalts were possibly derived from melting of the asthenosphere during oceanic lithospheric break-off and are not indicative of the oceanic crust. Some authors have favored a Late Jurassic closure time, mainly based on sedimentary or structural deformation studies (e.g., Li et al., 2017; Kapp et al., 2007; Huang et al., 2017; Zhang, 2004; Zhang et al., 2004; Ma et al., 2017). However, Guynn et al. (2006), based on the record of metamorphism, suggested that such a Jurassic closure event may just imply a collision between southern Qiangtang and another microcontinent rather than Lhasa-Qiangtang collision. In addition, the Bangong-Nujiang Ocean could have closed in a clockwise fashion from the Jurassic to Cretaceous, also based on studies of the regional metamorphism (Zhang et al., 2008) and paleomagnetism (Yan et al., 2016).

Here, we suggest that ascertaining whether oceanic subduction occurred during the Early Cretaceous is relevant to constraining the oceanic closure time. Arc-related magmatic rocks in a subduction setting, especially mafic rocks, have distinctive geochemical properties that distinguish them from those of other tectonic settings (e.g., Pearce and Peate, 1995). Therefore, we can potentially unveil the evolution of a subduction zone by identifying the arc rock associations.

However, due to the rare occurrence of Mesozoic mafic rocks in southern Qiangtang, previous studies have mainly focused on intermediate-felsic rocks (e.g., Hao et al., 2016a, 2016b; J.X. Li et al., 2014), which are not sensitive to the tectonic settings and thus may not provide solid and convincing evidence for arc magmatism, given that they may have their original distinctive tectonic settings obfuscated by fractional crystallization, mixing, and contamination processes or their arc geochemical characteristics may just be inherited from their crustal source rocks.

In this paper, we present new zircon U-Pb ages and Hf isotopic data, whole-rock major- and trace-element geochemical data, Sr-Nd-Hf isotopic compositions, and mineral geochemistry for the Gerze lavas, which contain basalt, basaltic andesite, andesite, dacite, and rhyolite, for a better understanding of the evolution of the Bangong-Nujiang Ocean. The results clearly show the arc affinities of the Early Cretaceous Gerze lavas, indicating that oceanic subduction may have lasted at least until ca. 100 Ma. Moreover, subduction of the Tethyan oceanic plateau during the Early Cretaceous is proposed for the first time to explain the evolution of the Bangong-Nujiang Ocean and the distinctive magmatism in southern Qiangtang.

GEOLOGIC SETTINGS AND PETROGRAPHIC CHARACTERISTICS

The Tibetan Plateau consists of the Songpan-Ganzi, northern Qiangtang, southern Qiangtang, Lhasa, and Himalaya blocks, from north to south (Fig. 1A; e.g., Yin and Harrison, 2000). These five blocks are separated by the Jinsha, LongmuCo-Shuanghu, Bangong-Nujiang, and Indus-Yalu-Zangpo suture zones, respectively. The Bangong-Nujiang suture zone is located in central Tibet, extending from the BangongCo in the west to the Nujiang River in the east, and it represents the remnant of the Bangong-Nujiang Ocean (Fig. 1B; e.g., Kapp et al., 2003). Complete sequences of ophiolites within the Bangong-Nujiang suture zone have been found in the Rutog, Dongco, Dongqiao, Amdo, and Dengqen areas (Wang et al., 2016). Late Mesozoic magmatic rocks (170–101 Ma) in southern Qiangtang (Fig. 1B) have been described in detail (e.g., Hao et al., 2016b; Liu et al., 2017; Kapp et al., 2003; Y.X. Zhang et al., 2017; Zhu et al., 2016) and are dominated by intermediate-felsic igneous rocks.

Our study area is located 30–60 km northeast in Gerze County (Fig. 1C), where there are Carboniferous, Permian, Triassic, Jurassic, Cretaceous, and Cenozoic strata. The Paleozoic, Triassic, and Jurassic strata are deformed and unconformably overlain by Cretaceous strata, which are unconformably overlain by Cenozoic strata. Here, we focused on the Cretaceous strata, which consist of the interbedded sedimentary rocks (sandstone, limestone, conglomerate, and calcareous shale) and volcanic rocks. The volcanic rocks cover an area of ~200 km^2, strike approximately E-W, and are mainly composed of lavas with minor volcanic breccia. Recently studied volcanic-sedimentary sections (Chen et al., 2017) have shown that the volcanic rocks are basalts, basaltic andesites, andesitic rocks, and rhyolites. Our samples from five sites (sites a to e in Fig. 1C) cover lavas from basalts to rhyolites. The field relationships are presented in Supplementary Material 1 in the GSA Data Repository.[1]

The Gerze basalts and andesites are from site a. The basalts show an intergranular texture with coarse phenocrysts of clinopyroxene and plagioclase (Fig. 2A). They have alteration products of epidote and calcite. The andesites are porphyritic with phenocrysts of coarse- and medium-grained plagioclase and minor quartz (Fig. 2B). The alteration minerals in the andesites are also mainly epidote and calcite. The Gerze basaltic andesites are from site b. They have a porphyritic texture with fine phenocrysts of plagioclase (Fig. 2C). The alteration minerals (calcites and minor dolomites) can be observed in thin sections of the basaltic andesites. The Gerze dacites are from sites c and d. They also show a porphyritic texture with phenocrysts of plagioclase. The Gerze rhyolites are from site e and are relatively fresh. They are porphyritic with phenocrysts of medium-grained plagioclase and minor quartz (Fig. 2D).

RESULTS

Whole-rock major- and trace-element and Sr-Nd-Hf isotope analyses, secondary ion mass spectrometry (SIMS) zircon U-Pb dating, and mineral chemical analyses were conducted at the State Key Laboratory of Isotope Geochemistry, Guangzhou Institute of Geochemistry, Chinese Academy of Sciences (CAS), Guangzhou, China. Laser ablation–inductively coupled plasma–mass spectrometry (LA-ICP-MS) zircon U-Pb dating and Hf isotope analyses were conducted at the Institute of Geology and Geophysics, CAS. A more detailed discussion of the methodology can be found in Supplementary Material 2 (see footnote 1; e.g., Huang et al., 2007; Li et al., 2006, 2007, 2010; Wu et al., 2006; Xie et al., 2008), and the analytical results are presented in Supplementary Material 3–7 (see footnote 1).

Ages of Gerze Lavas

The Gerze lavas in the Cretaceous strata were previously suggested to have erupted during 110–104 Ma (Fig. 1C) based on the ages of the rhyolites (ca. 110 Ma; Chang et al., 2011; Kapp et al., 2005) and the basaltic andesites (ca. 104 Ma; Chen et al., 2017). Here, we present new LA-ICP-MS zircon U-Pb ages for the Gerze dacites and a SIMS U-Pb age for the Gerze basalts (Fig. 3; Supplementary Material 5–6 [see footnote 1]).

[1]GSA Data Repository item 2018295, the analytical methods and results for the Gerze lavas from central Tibet, is available at http://www.geosociety.org/datarepository/2018 or by request to editing@geosociety.org.

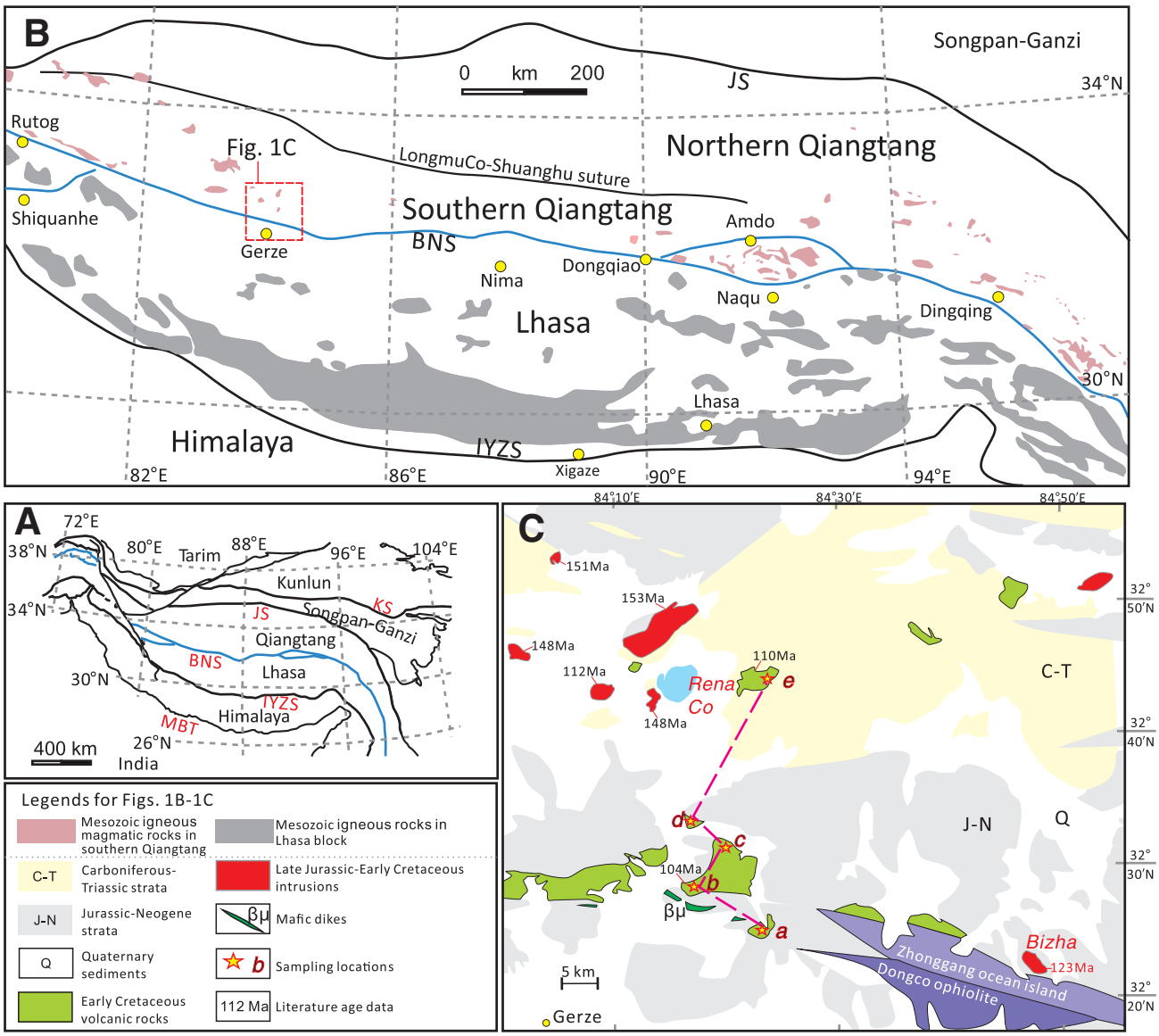

Figure 1. (A) Tectonic framework of the Tibetan Plateau (modified after Yin and Harrison, 2000), showing main suture zones between the major blocks: KS—Kunlun suture; JS—Jinsha suture; BNS—Bangong-Nujiang suture; IYZS—Indus-Yarlung-Zangpo suture. MBT—Main Boundary Thrust. (B) Simplified geological map showing the Mesozoic magmatism in southern Qiangtang and Lhasa (after Liu et al., 2017). (C) Geological map of the studied area, Gerze County. Sampling site a for basalts (QT04-1, QT04-2) and andesites (QT03-1, QT03-2); site b for basaltic andesites (ZB78-1 to ZB78-4); sites c and d for dacites (c for GZ26-1 and GZ26-2; d for GZ01-1); and site e for rhyolites (ZB79-1 to ZB79-4). Literature age data are from Hao et al. (2016a), Chen et al. (2017), Chang et al. (2011), and Kapp et al. (2005). Bizha diorites are located to the east of the Gerze and have been studied by Hao et al. (2016b).

Most of the zircons from the Gerze dacites show clear oscillatory zoning and have variable grain sizes of ~50–250 μm and length-to-width ratios of 1:1–3:1. These zircons have high Th/U ratios (0.2–1.7), with U and Th concentrations of 114–760 ppm and 72–366 ppm, respectively, indicating a magmatic origin (Belousova et al., 2002). Gerze dacite samples GZ01-1 and GZ26-1 have concordant $^{206}Pb/^{238}U$ ages with weighted mean ages of 105.6 ± 1.2 Ma (mean square of weighted deviates [MSWD] = 1.6) and 105.6 ± 1.3 Ma (MSWD = 1.8), respectively (Figs. 3A and 3B).

It should be noted that basalts may contain very few or no magmatic zircons but many xenocrystic grains, and we should use their zircon ages with caution. Indeed, zircons of the Gerze basalt sample (QT04-1) yielded variable U-Pb ages with peaks mainly at 150 and 108 Ma (Fig. 3C). The ca. 150 Ma zircons may be xenocrystic grains, given their similarities with those from the coeval intrusions in the Gerze area (Fig. 1C; Hao et al., 2016a). However, the younger zircons with a weighted mean age of 107.7 ± 1.9 Ma (Fig. 3C) differ from those of the coeval intrusions and the nonbasaltic lavas in the Gerze area (Fig. 1C) by their short prismatic shape and high Th (206–683 ppm) and U (419–1114 ppm) contents. Indeed, these zircons are more likely to have a mafic magmatic

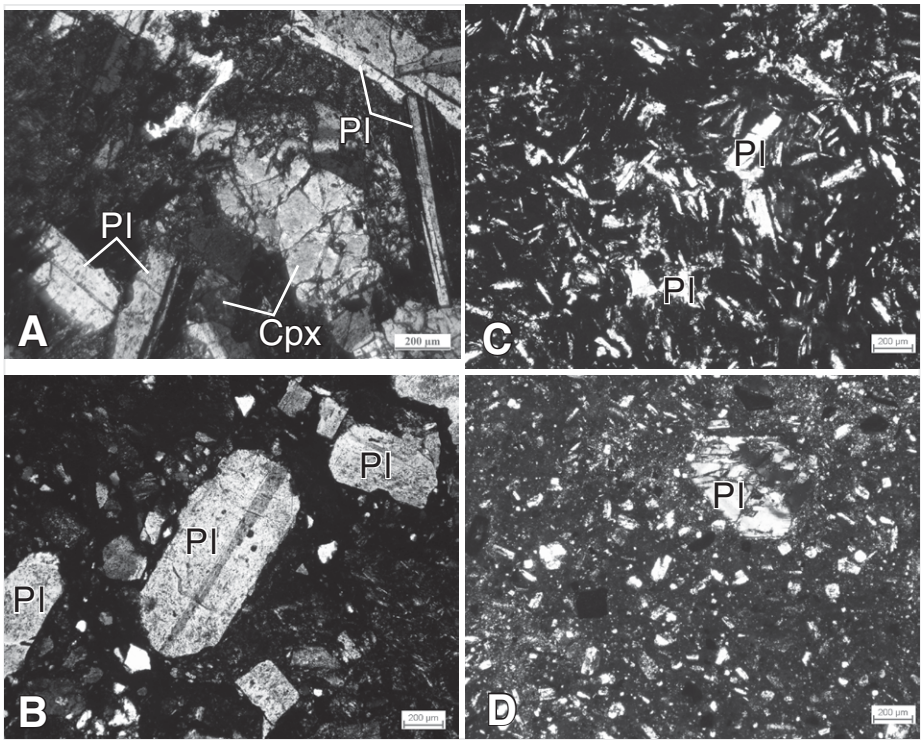

Figure 2. Representative thin section photomicrographs of the Gerze lavas. (A) basalt QT04-1; (B) andesite QT03-2; (C) basaltic andesite ZB78-3; (D) rhyolite ZB79-1. Mineral abbreviations: Cpx—clinopyroxene; Pl—plagioclase.

signature and may have crystallized from the basaltic magmas (Wang et al., 2008; Tang et al., 2017; Hoskin and Schaltegger, 2003). Moreover, this age is consistent with the age range of other Gerze lavas. Thus, we suggest that this age of 108 Ma currently provides the best age estimate for the Gerze basalts. Therefore, the Gerze lavas within the Cretaceous strata were formed at 110–104 Ma.

Mineral and Whole-Rock Geochemistry

Rock Classification

The Gerze lavas have variable and high loss on ignition values (LOI) of 1.9–8.4 wt%, indicating that some samples could have been altered, consistent with field and petrographic observations (e.g., presence of calcites) and mineral chemical compositions. Consequently, the major elements were recalculated on an anhydrous basis. In addition, for the altered igneous rocks, potential element mobility limits the use of standard classification diagrams, such as the total alkali-silica and K_2O-SiO_2 diagrams (Peccerillo and Taylor, 1976; Le Bas et al., 1986). Therefore, we employed another nomenclature diagram using immobile elements, like Co versus Th (Hastie et al., 2007), wherein the Gerze lavas plot in a wide range from basalt to rhyolite (Fig. 4), consistent with their SiO_2 contents (volatile-free) of 49.2–74.2 wt%. Using their mineral assemblages and major- and trace-element and isotopic compositions, we divided the Gerze lavas into five types of volcanic rocks, i.e., basalts, basaltic andesites, andesites, dacites, and rhyolites.

Mineral Compositions

The clinopyroxene grains in the Gerze basalts are relatively fresh, with SiO_2, CaO, FeO, and MgO contents (in wt%) of 48.7–53.2, 20.0–21.5, 5.9–11.6, and 12.6–16.9, respectively (Supplementary Material 7 [footnote 1]). They have variable Mg# values of 66–84, where Mg# = molar MgO/(MgO + FeO) × 100. The plagioclase phenocrysts in the Gerze basalts, basaltic andesites, andesites, and dacites are significantly altered and do not retain their original chemical compositions. They generally have undergone Ca and Al losses but gained Si and Na. For instance, the plagioclases in the Gerze basalts, basaltic andesites, and andesites have extremely low CaO contents (<0.5 wt%) and SiO_2, Al_2O_3, and Na_2O (in wt%) compositions of 68.8–71.5, 18.9–20.2, and 8.5–10.5; 71.5–73.2, 19.6–20.4, and 7.1–9.7; and 69.1–71.9, 20.0–21.2, and 7.8–9.5, respectively (Supplementary Material 7 [footnote 1]). In contrast, the plagioclases in the rhyolites are relatively fresh and exhibit SiO_2, Al_2O_3, Na_2O, and CaO contents (in wt%) of 54.5–59.5, 25.3–27.4, 5.7–7.3, and 8.1–11.4, respectively.

Mineral chemistry can be used to evaluate the degree of alteration of a rock. If the volcanic rocks have been significantly affected by alteration, the main mineral phases will not retain their igneous signatures and chemical compositions. Therefore, the Gerze basalts, basaltic andesites, andesites, and dacites have undergone significant posteruptive alteration, whereas the Gerze rhyolites have not been significantly altered.

Alteration Effects

Previous geochemical studies on altered igneous rocks have demonstrated that the majority of large ion lithophile elements (LILEs) can be variably mobilized, whereas the high field strength elements (HFSEs), rare earth elements (REEs), and transition elements are considered to be relatively immobile during a range of weathering, hydrothermal, and low-grade metamorphic processes (e.g., Hastie et al., 2007, 2011). Hence, the effects of posteruptive alteration on elemental mobility need to be assessed prior to the interpretation of geochemical data. Representative variation diagrams for the Gerze lavas are shown wherein incompatible elements are plotted against immobile Nb (Fig. 5). If the elements are immobile, the data should form positive linear vectors on log-log plots (e.g., Hastie et al., 2011; Pearce, 2014).

For the Gerze basalts, the bivariate diagrams of LILEs (Sr and Ba) versus Nb show large scatter without pre-alteration positive linear trends (Figs. 5A and 5B), suggesting such elements are mobile and cannot be used to characterize rock geochemistry and to decipher petrogenesis. Conversely, Th, Zr, La, Nd, Y, and Yb show much smaller scatter and correlate significantly with Nb, indicating that these elements are relatively immobile (Figs. 5C–5H). As for the Gerze basaltic andesites, except for Ba, elements including Sr, Th, Zr, La, Nd, Y, and Yb correlate tightly with Nb, indicating their immobility (e.g., Hastie et al., 2011; Pearce, 2014). Figure 5 also shows that most trace elements of the Gerze andesites and dacites have tight correlation with Nb, indicating these elements have not been affected much by alteration. The Gerze rhyolites have fresh plagioclases and the lowest LOI values of 1.9–2.1 wt%, indicating that they were probably the least affected among the Gerze lavas during alteration.

Gerze Basalts and Basaltic Andesites

The Gerze basalts have SiO_2 contents of 49.2–50.9 wt% and low MgO (4.7–6.0 wt%), Cr (24–180 ppm), and Ni (43–91 ppm) contents.

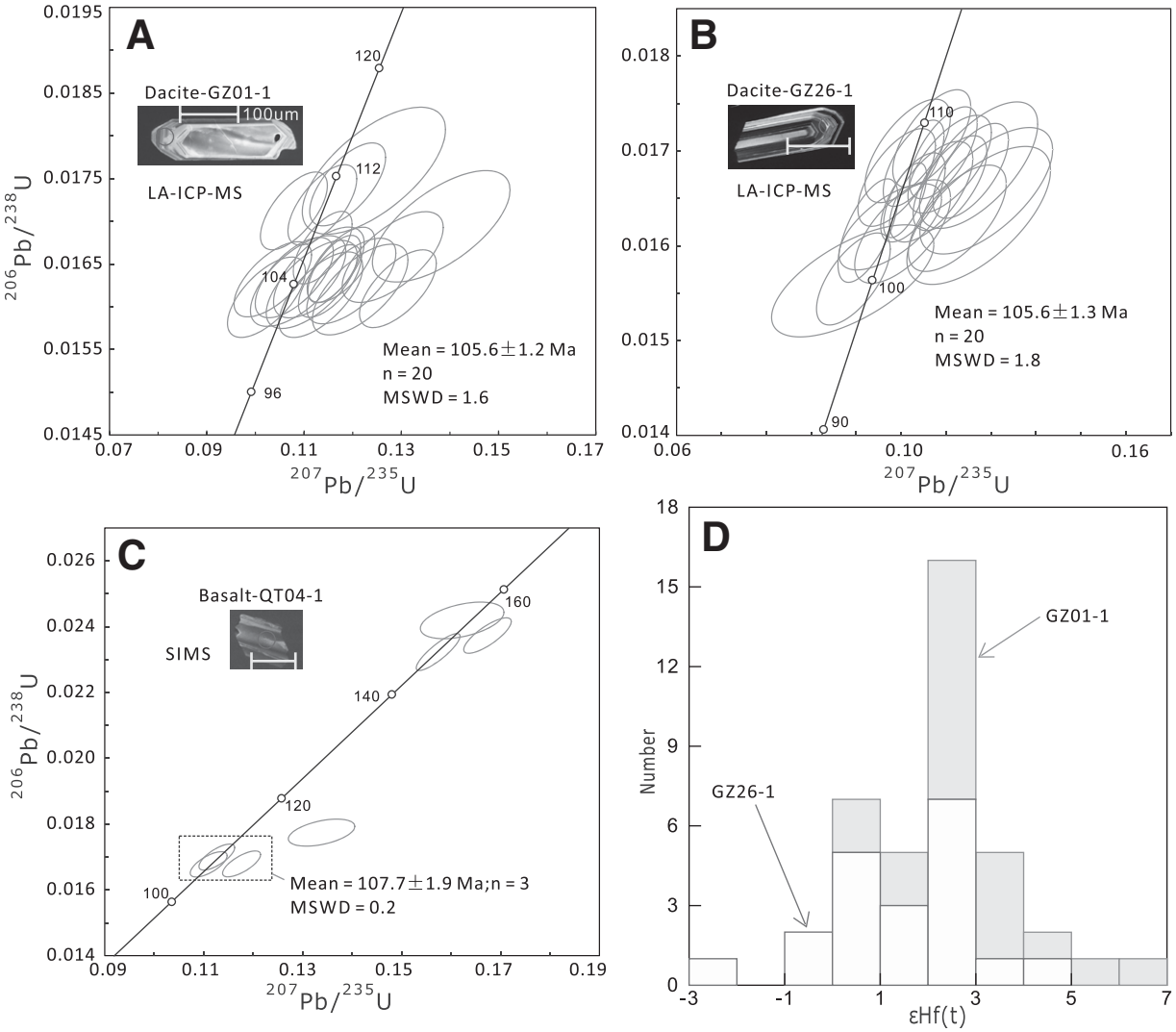

Figure 3. Zircon U-Pb concordia diagrams with representative zircon cathodoluminescence (CL) images for the Gerze lavas: (A–B) laser ablation–inductively coupled plasma–mass spectrometry (LA-ICP-MS) dating results of dacites GZ01-1 and GZ26-1, respectively, and (C) secondary ion mass spectrometry (SIMS) dating result of basalt QT04-1. (D) Histogram of zircon Hf isotopes for the Gerze dacites. MSWD—mean square of weighted deviates.

The Gerze basalts show subparallel REE distribution patterns yet variable LILEs (e.g., Sr, Ba, U; Figs. 6A–6B), consistent with the mobility of the latter. They are characterized by low total REE contents and slightly depleted light (L) REEs [$(La/Yb)_N$ = 0.66–0.69, where N denotes normalized to chondrite values of Sun and McDonough, 1989] and flat heavy (H) REEs [$(Gd/Yb)_N$ = 1.0–1.1], very similar to the average normal mid-ocean-ridge basalt (N-MORB; Fig. 6A). The Gerze basalts show extremely depleted Nd and Hf isotopic compositions [$\varepsilon_{Nd}(t)$ = 8.5–9.0; $\varepsilon_{Hf}(t)$ = 17.19–17.20]. Nd and Hf are immobile during alteration processes, and thus their isotope systems could represent the primary composition of the Gerze basalts. The high Sr isotopic values [$(^{87}Sr/^{86}Sr)_i$ = 0.7069–0.7071] of the Gerze basalts, deviating from the mantle array (Fig. 7), are meaningless, because Sr has been mobilized by alteration processes.

Relative to the Gerze basalts, the Gerze basaltic andesites, with SiO_2 = 52.0–59.0 wt% and MgO = 1.2–2.5 wt%, show distinct REE distribution patterns with higher total REE contents and slight LREE enrichments [$(La/Yb)_N$ = 3.3–4.0; Fig. 6C]. The Gerze basaltic andesites exhibit some arc-like geochemical signatures, e.g., negative Nb and Ta anomalies (Fig. 6D). However, they differ from the majority of arc basalts and basaltic andesites by higher HFSEs contents [e.g., Nb (10–12 ppm), Ta (0.7–0.8 ppm), Zr (296–323 ppm)], and elevated Nb/La (>0.5) ratios. The Gerze basaltic andesite also have high TiO_2 (1.9–2.2 wt%) and P_2O_5 (0.37–0.42 wt%) contents. The basaltic andesites show depleted Sr-Nd isotopic compositions with $\varepsilon_{Nd}(t)$ = 2.5–2.7 and $(^{87}Sr/^{86}Sr)_i$ = 0.7047–0.7050 (Fig. 7).

Gerze Andesites and Dacites

Two andesite samples show subparallel REE and trace-element distribution patterns (Figs. 6E–6F). The Gerze andesites show weak LREE enrichments [$(La/Yb)_N$ = 2.7–3.1] with relatively low REE contents and negligible Eu anomalies (Eu/Eu* = 0.90–0.93). The Gerze andesites have relatively enriched Sr-Nd isotopic compositions, with $\varepsilon_{Nd}(t)$ = –3.3 to –2.9 and $(^{87}Sr/^{86}Sr)_i$ = 0.7095–0.7096 (Fig. 7).

In contrast, the Gerze dacites are characterized by high REE contents, significant LREE enrichments [$(La/Yb)_N$ = 12–13], and negative

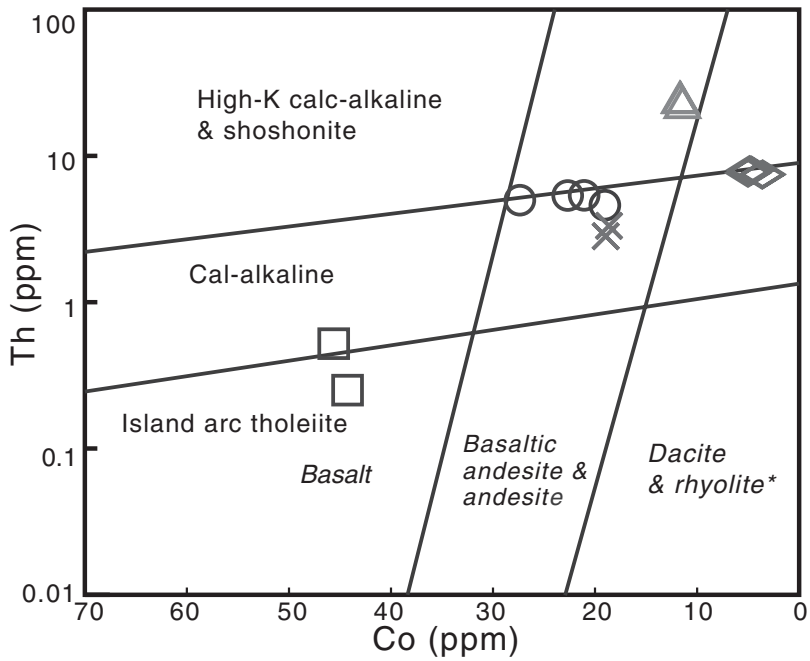

Figure 4. Th-Co discrimination diagrams for the Gerze lavas (Hastie et al., 2007), where asterisk (*) indicates latites and trachytes that also fall in the dacite and rhyolite fields.

Eu (Eu/Eu* = 0.46–0.47) and Sr anomalies (Figs. 6E–6F). The Gerze dacites have similar Nd but lower Sr isotopic ratios [$\varepsilon_{Nd}(t)$ = –3.5 to –3.3 and $(^{87}Sr/^{86}Sr)_i$ = 0.7062–0.7066] relative to the Gerze andesites (Fig. 7). Magmatic zircons from the dacite samples GZ01-1 and GZ26-1 yielded $\varepsilon_{Hf}(t)$ values of +0.3 to +6.5 and of –2.5 to +4.1, respectively (Fig. 3D).

Gerze Rhyolites

The Gerze rhyolites have relatively constant and high SiO_2 (73.4–74.2 wt%) but low MgO (0.8–0.9 wt%) contents. The Gerze rhyolites show clear REE fractionation [$(La/Yb)_N$ = 24–29] with slightly concave middle and heavy REE patterns, and weak negative Eu anomalies (Eu/Eu* = 0.86–0.90; Fig. 6G). The Gerze rhyolites have high La (16.6–18.2 ppm) and low Y and Yb (4.4–5.8 and 0.4–0.5 ppm, respectively) contents, giving high La/Yb ratios (20–124). These geochemical characteristics seem to be similar to those of classic adakites (e.g., Drummond et al., 1996; Martin et al., 2005; Condie, 2005) but distinct from those of normal arc andesite-dacite-rhyolite (ADR) suites. However, the Gerze rhyolites differ from typical adakites by relatively higher SiO_2 (>70 wt%) and lower MgO (<2 wt%) and transition element (Cr and Ni) contents. Moreover, the lower Sr contents (299–343 ppm) and Sr/Y ratios could distinguish the Gerze rhyolites from classic adakites. Typical Cenozoic adakites are intermediate-silicic volcanic and intrusive rocks with SiO_2 >56 wt%, Al_2O_3 >15 wt%, MgO <6 wt%, Y <18 ppm, Yb <1.9 ppm, and Sr >400 ppm, which are widely considered to be generated by partial melting of basaltic rocks with residues of garnet amphibolite, amphibole-bearing eclogite, or eclogite (Defant and Drummond, 1990). The Gerze rhyolites show slightly depleted Sr-Nd isotopes [$\varepsilon_{Nd}(t)$ = 0.9–1.3, $(^{87}Sr/^{86}Sr)_i$ = 0.7049–0.7050; Fig. 7].

DISCUSSION

Petrogenesis of Gerze Lavas

With the previous assessments of potential alteration effects, we can selectively use immobile elements and resistant isotope systems to discuss the petrogenesis of the Gerze lavas.

Gerze Basalts

The extremely depleted Nd-Hf isotopes [$\varepsilon_{Nd}(t)$ = 8.5–9.0; $\varepsilon_{Hf}(t)$ = 17.19–17.20] of the Gerze basalts probably imply that they have not been significantly contaminated by crustal components during their ascent to the continental crust.

The Gerze basalts have MgO of 4.7–6.0 wt%, Cr of 24–180 ppm, and Ni of 43–91 ppm, clearly lower than those of mantle-derived primary melts (MgO >8 wt%, Cr >1000 ppm, and Ni >400 ppm). This suggests that the Gerze basalts underwent a certain degree of fractional crystallization of mafic minerals (e.g., olivine, clinopyroxene) from parental magmas. This is consistent with the chemical compositions of clinopyroxene phenocrysts having variable and low Mg# (66–84). Fractional crystallization (FC) without assimilation (A) during basaltic magma differentiation would not change the REE distribution patterns and isotopes. The Gerze basalts show depleted LREEs and flat HREEs, very similar to N-MORB. Thus, this probably indicates that they originated from an asthenosphere mantle, consistent with their extremely depleted Nd-Hf isotopic compositions. In addition, the Gerze basalts have comparable Nd isotopes to the N-MORBs of the Bangong-Nujiang suture zone ophiolites. Also, Li et al. (2015) suggested that the Duolong diabases with whole-rock $\varepsilon_{Nd}(t)$ of 7.3–9.1 and zircon $\varepsilon_{Hf}(t)$ of 14.8–16.1 should have originated from the depleted asthenospheric mantle. Therefore, the REE distribution patterns and Nd-Hf isotopes of the Gerze basalts strongly indicate that they were sourced from the depleted asthenospheric mantle. It should be noted that the Gerze basalts similar to N-MORB may not be fragments of the Bangong-Nujiang oceanic crust, though there are many ophiolites nearby (Fig. 1C), because the mafic rocks within these ophiolites are dominated by Cretaceous oceanic-island basalts (OIBs; e.g., Zhonggong and Dongco; Bao et al., 2007). Moreover, recent studies have suggested that most of the ophiolitic fragments across the Bangong-Nujiang suture zone were derived dominantly from two oceanic plateaus with peak ages at 185 Ma and 121 Ma (K.J. Zhang et al., 2014) and some N-MORB–type ophiolites that mainly occurred during the Jurassic (Wang et al., 2016).

However, the Th enrichment of the Gerze basalts could imply some subduction inputs into their mantle source. Th/Nb can effectively indicate subduction input because the Th/Nb ratio retains an almost-constant value during mantle melting, whereas the mobile element Th and immobile element Nb can be clearly decoupled during subduction. Therefore, the Th/Yb versus Nb/Yb discrimination diagram based on the Th/Nb proxy (e.g., Pearce, 2014) can be used to identify subduction inputs into the mantle source. Lavas from nonsubduction settings plot along a MORB-OIB array, while lavas derived from subduction-modified mantle are displaced from the mantle array to higher Th/Yb ratios (Fig. 8A). The Gerze basalts have higher Th/Nb and clearly deviate from the mantle array (Fig. 8A), suggesting a subduction-modified mantle source. Moreover, the Gerze basalts have similar Nb/Yb but higher Th/Yb relative to

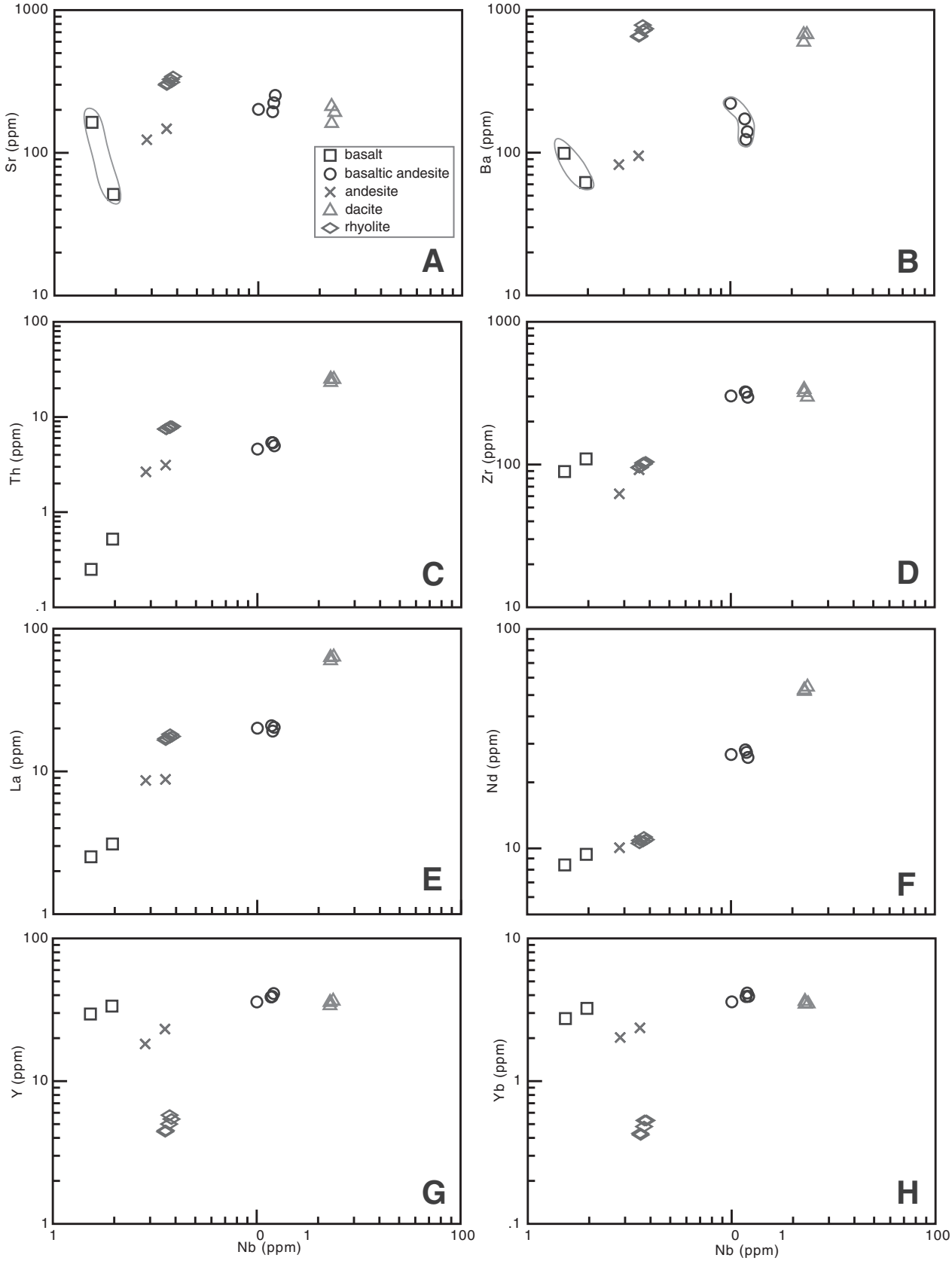

Figure 5. Variation diagrams for a range of incompatible elements plotted against Nb for the Gerze lavas to assess the alteration effects on different elements.

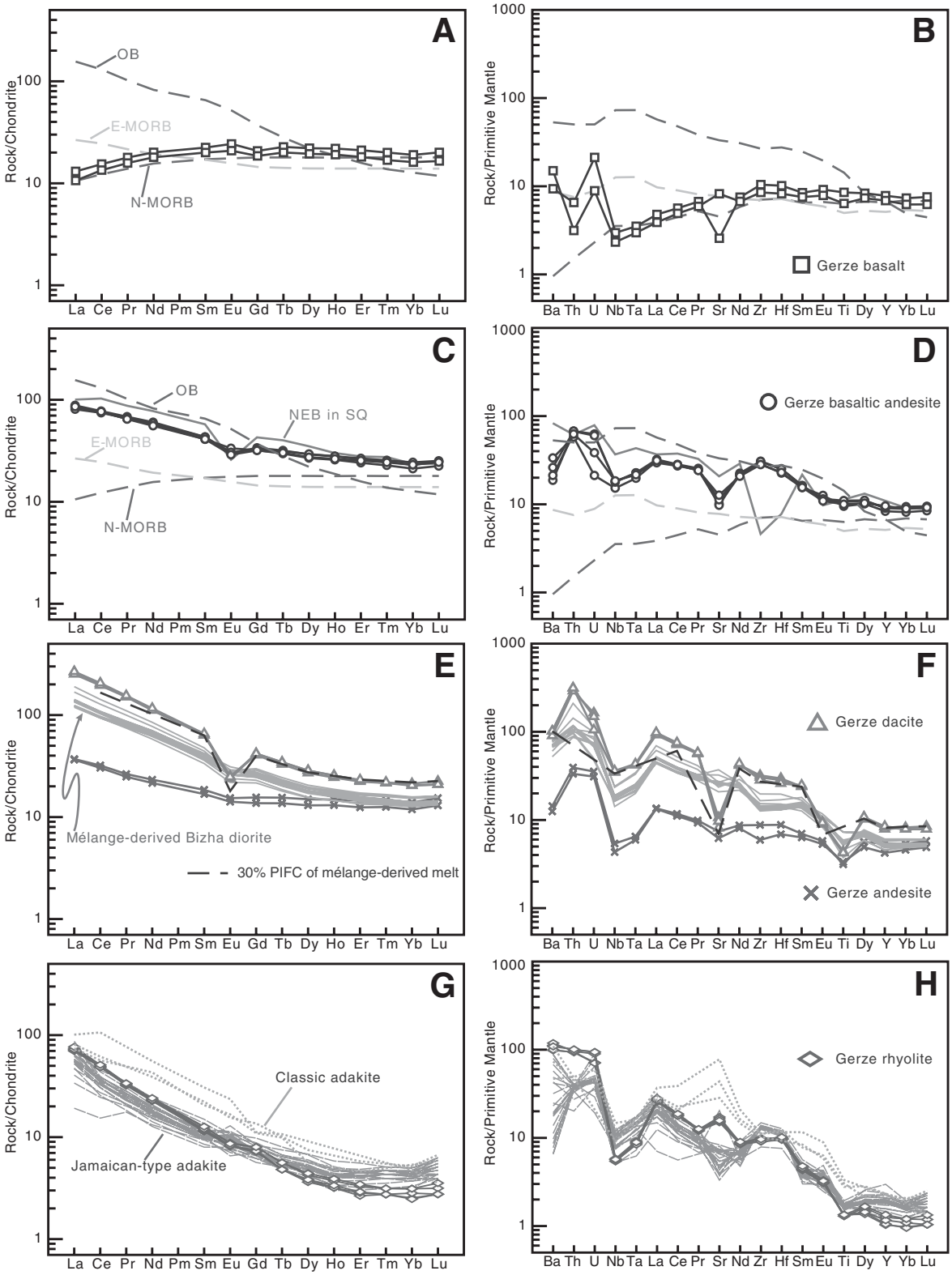

Figure 6. Chondrite-normalized rare earth element (REE) patterns and primitive mantle–normalized trace-element diagrams for Gerze basalts (A–B), basaltic andesite (C–D), andesites and dacites (E–F), and rhyolites (G–H). The values of chondrite, normal mid-ocean-ridge basalt (N-MORB), enriched mid-ocean-ridge basalt (E-MORB), and oceanic-island basalt (OIB) are from Sun and McDonough (1989). Normalizing primitive mantle is from McDonough and Sun (1995). The gabbroic enclave (Nb-enriched basalt [NEB]) in southern Qiangtang (SQ) is from S.M. Li et al. (2014). The mélange-derived Bizha diorites are from Hao et al. (2016b). Partition coefficients for plagioclase crystallization fractionation (PlFC) are from Rollinson (1993). Jamaican-type adakites (JTA) are from Hastie et al. (2011, 2015). The typical adakites are from Drummond et al. (1996), Martin et al. (2005), and Condie (2005).

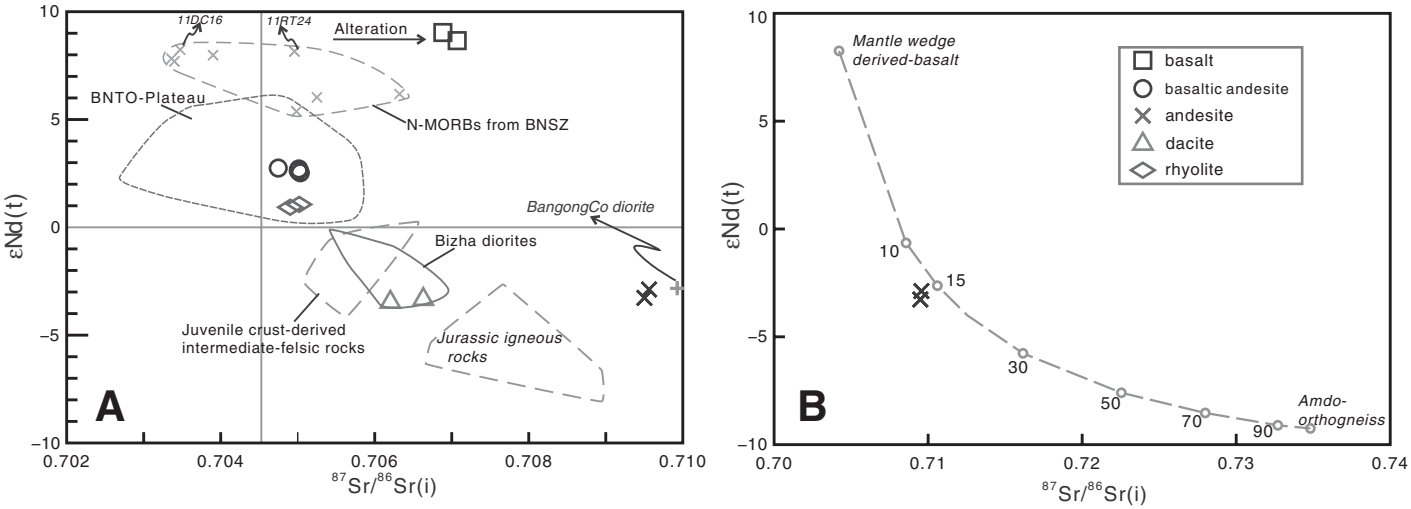

Figure 7. (A) Sr-Nd isotopes for the Gerze lavas. All Sr-Nd isotopic ratios are corrected to 110 Ma. Normal mid-ocean-ridge basalts (N-MORBs) of Bangong-Nujiang suture zone (BNSZ) are from Wang et al. (2016), and oceanic plateau basalts are from Bao et al. (2007), K.J. Zhang et al. (2014), Zhu et al. (2006), and Wang et al. (2016). BNTO—Bangong-Nujiang Tethyan Ocean. Juvenile crust–derived intermediate-felsic rocks include the Early Cretaceous Duolong porphyries (Li et al., 2013) and RenaCo adakitic granodiorite porphyries (Hao et al., 2016a). Jurassic igneous rocks include the ChaerkangCo (Y.X. Zhang et al., 2017) and RenaCo plutons (Hao et al., 2016a). The Bizha diorites are from Hao et al. (2016b). The BangongCo diorite is from Liu et al. (2014). (B) Simple isotope modeling to estimate the contributions of the basalts and ancient crust in generating the Gerze andesites. Sr-Nd isotopes of mantle wedge–derived basalts are from average compositions of two N-MORBs, 11RT24 and 11DC16, with values of Sr = 102 ppm, Nd = 3 ppm, $\varepsilon_{Nd}(t)$ = 8.2, and $(^{87}Sr/^{86}Sr)_i$ = 0.7042. Amdo orthogneisses are from Harris et al. (1988) with the average compositions of Sr = 152 ppm, Nd = 28 ppm, $\varepsilon_{Nd}(t)$ = –9.3, and $(^{87}Sr/^{86}Sr)_i$ = 0.7348.

N-MORB, suggesting slab fluid inputs into their mantle source.

Therefore, partial melting of depleted asthenospheric mantle metasomatized by slab fluids and subsequent fractional crystallization likely contributed to the generation of the Gerze basalts.

Gerze Basaltic Andesites: Nb-Enriched Basalts

Although the Gerze basaltic andesites have higher Th/Nb values and also show arc affinities, they probably do not share a mantle source with the Gerze basalts. The Gerze basaltic andesites have LREE enrichments and exhibit REE distribution patterns distinct from those of the Gerze basalts. In addition, the Gerze basaltic andesites have different Nd isotope values (Fig. 7A) and La/Sm ratios (Fig. 8B) compared to the Gerze basalts. Thus, FC processes in the parental magmas of the Gerze basalts could not have formed the Gerze basaltic andesites. Moreover, the Gerze basaltic andesites could not be produced by AFC processes in the parental magmas of the Gerze basalts, because crustal assimilation would strongly decrease the Nb/La ratios with decreasing Nd. Nevertheless, some Gerze basaltic andesites have similar Nb/La ratios compared to the Gerze basalts, but they have clearly lower Nd isotopes (Fig. 8C), which is inconsistent with crustal assimilation.

We suggest that the Gerze basaltic andesites had a mantle source distinct from that of the Gerze basalts. In fact, the high TiO_2 and P_2O_5 contents (1.9–2.2 and 0.37–0.42 wt%, respectively), high HFSE contents [Nb (10–12 ppm), Ta (0.7–0.8 ppm), Zr (296–323 ppm)], and elevated Nb/La ratios (>0.5) of the Gerze basaltic andesites distinguish them from normal arc basaltic rocks derived from subduction fluid–modified mantle wedge, but these values resemble closely those of the Nb-enriched basaltic rocks, such as the Sulu arc basalts and basaltic andesites in southern Philippines (Fig. 8D; Castillo et al., 2007). Moreover, the Gerze basaltic andesites show similar REE and trace-element distribution patterns to the Jurassic Nb-enriched basalts (gabbroic enclaves) in southern Qiangtang (Figs. 6C–6D; S.M. Li et al., 2014).

Given that Nb-enriched basalts have been distinguished from high-Nb basalts in the Sulu arc based on the high-Nb basalts being more enriched in LILEs, LREEs, Nb, and Ta (Castillo et al., 2007), the terms high-Nb basalts and Nb-enriched basalts should not be used interchangeably. Here, we adopt the terminology of identifying Nb-enriched basalts and high-Nb basalts with Nb contents of 5–20 ppm and >20 ppm, respectively (e.g., Hastie et al., 2011). Thus, the Gerze basaltic andesites should be classified as Nb-enriched basalts.

Two alternative mantle sources have been popularly proposed to account for the origin and distinctive geochemical characteristics of Nb-enriched basalts and high-Nb basalts: (1) upper mantle composed of enriched OIB-like and depleted N-MORB–type components (e.g., Castillo et al., 2002, 2007; Hastie et al., 2015); and (2) mantle wedge that has been metasomatized by slab melts (Sajona et al., 1996; Hastie et al., 2011).

Hastie et al. (2011) suggested that the Halberstadt high-Nb basalts in Jamaica can be divided into two compositional subgroups, and Hastie et al. (2015) further proposed that the group 1 high-Nb basalts were derived from mantle source 1, whereas the group 2 high-Nb basalts originated from mantle source 2. The detailed modeling results in Hastie et al. (2015) showed that small degrees of partial melting of mantle source 1 can produce the group 1 high-Nb basalts. With larger degrees of partial melting, the modeled partial melts can replicate the elevated HREE patterns of the group 2 high-Nb basalts, but with clearly higher LREEs and middle (M) REEs than the group 2 high-Nb basalts. This probably suggests that partial melting of mantle source 1 could yield high-Nb basalts with striking REE fractionation that cannot be obliterated

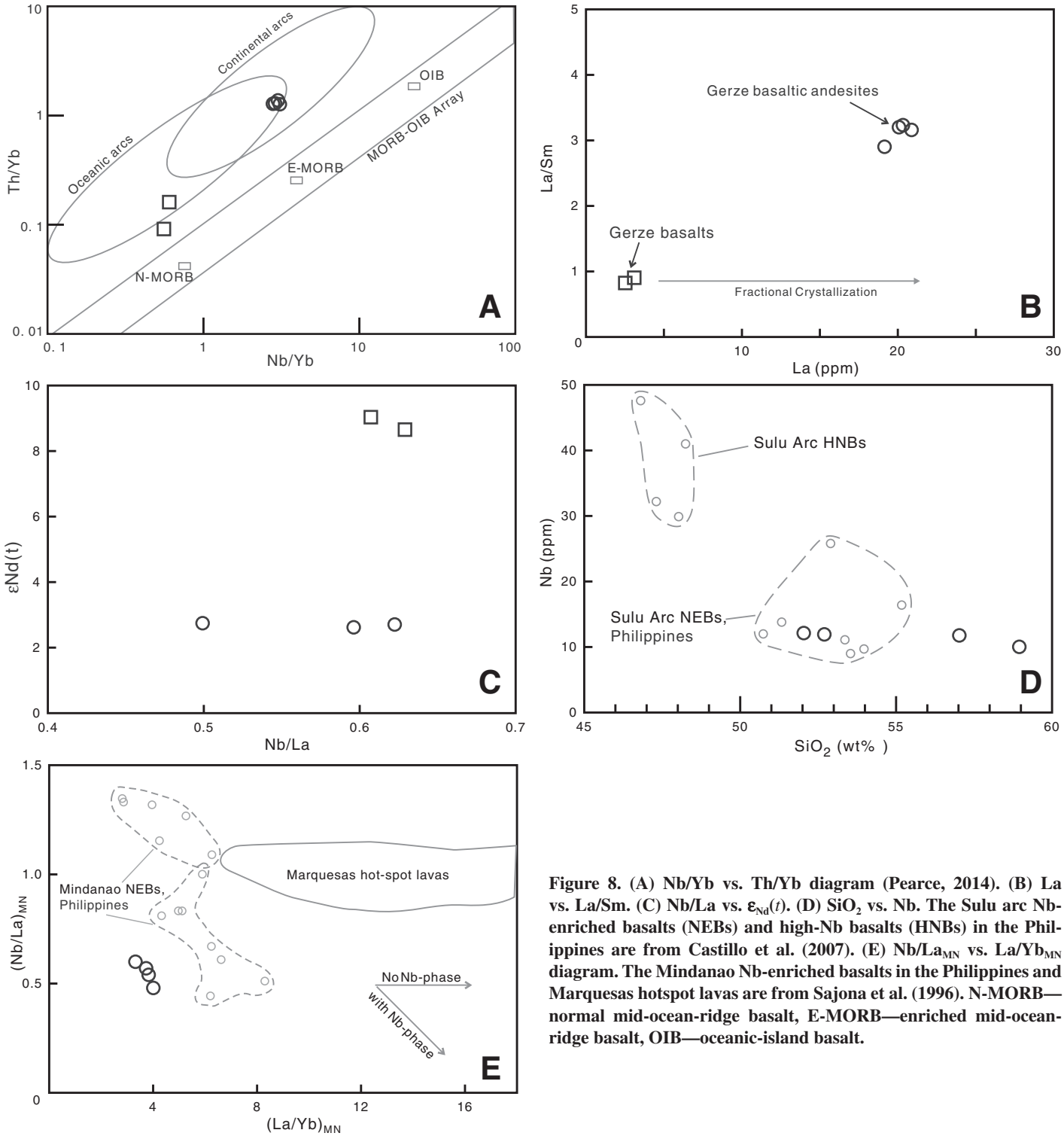

Figure 8. (A) Nb/Yb vs. Th/Yb diagram (Pearce, 2014). (B) La vs. La/Sm. (C) Nb/La vs. $\varepsilon_{Nd}(t)$. (D) SiO_2 vs. Nb. The Sulu arc Nb-enriched basalts (NEBs) and high-Nb basalts (HNBs) in the Philippines are from Castillo et al. (2007). (E) Nb/La_{MN} vs. La/Yb_{MN} diagram. The Mindanao Nb-enriched basalts in the Philippines and Marquesas hotspot lavas are from Sajona et al. (1996). N-MORB—normal mid-ocean-ridge basalt, E-MORB—enriched mid-ocean-ridge basalt, OIB—oceanic-island basalt.

completely by variable degrees of partial melting. This is consistent with the residual garnets in mantle source 1. The Gerze Nb-enriched basalts have insignificant REE fractionation with Sm/Yb ratios clearly lower than those of the Halberstadt group 2 high-Nb basalts, indicating that they are not products of partial melting of mantle source 1.

Recently, Li et al. (2016) reported some OIB-type rocks with positive Nb-Ta-Ti anomalies in the Gerze area and suggested that they were likely derived from the upwelling garnet-asthenosphere mantle through a slab window in the mantle wedge. A mantle source involving such OIB-like components would also produce higher Sm/Yb ratios in the resultant high-Nb basalts and Nb-enriched basalts, in contrast to the Gerze Nb-enriched basalts. Moreover, such

OIBs have slightly higher Nd isotopes than the Gerze Nb-enriched basalts (Li et al., 2016). Thus, upper mantle composed of such OIB-like and extremely depleted N-MORB–type components could not be the mantle source of the Gerze Nb-enriched basalts.

Accordingly, mantle source 2 (i.e., mantle wedge that has been metasomatized by slab melts) could be plausibly invoked as the origin of the Gerze Nb-enriched basalts. In this model, slab melts migrating through a mantle wedge will hybridize and metasomatize the mantle peridotite to precipitate Nb- and Ti-enriched phases (dominantly amphibole) in the mantle source (e.g., Sajona et al., 1996; Hastie et al., 2011). The amphiboles will subsequently break down by convection, thus promoting partial melting of the mantle wedge and generation of Nb-enriched basalts. Sajona et al. (1996) suggested that the diagram of $(Nb/La)_{MN}$ versus $(La/Yb)_{MN}$ (where MN denotes normalized to primitive mantle values of Sun and McDonough, 1989) can identify the presence of Nb-bearing phases (e.g., amphiboles) in the mantle source. Nb/La would not vary with degree of melting when no Nb-bearing phases were in the mantle, given Nb and La have similar bulk distribution coefficients, but products of partial melting would form negative-sloping trends if Nb-enriched phase were involved in this process (Fig. 8E). In this respect, the Gerze Nb-enriched basalts clearly show a negative trend (Fig. 8E), similar to the scenarios proposed for the Nb-enriched basalts in Mindanao, Philippines (Sajona et al., 1996), suggesting their origination from slab melt-metasomatized mantle wedge with Nb-bearing phases.

Gerze Dacites and Andesites

The significant differences in REE and trace-element distribution patterns between the Gerze andesites and dacites imply different origins.

The Gerze dacites show significant negative Eu and Sr anomalies, probably indicating fractionation of plagioclases during their formation. The distinct REE distribution patterns and isotopes of the Gerze dacites from the Gerze basalts and Nb-enriched basalts likely preclude their parental magmas from being the Gerze basaltic magmas. Instead, the Gerze dacites exhibit REE and trace-element distribution patterns parallel to the Bizha diorites (Figs. 6E–6F), except for their evidently negative Sr and Eu anomalies. In addition, the Gerze dacites and Bizha diorites have similar Sr-Nd isotopic compositions (Fig. 7A). Furthermore, the zircon $\varepsilon_{Hf}(t)$ (–2.5 to +6.5) values of the Gerze dacites (Fig. 3D) are very close to those of the Bizha diorites (–5.3 to +3.6; Hao et al., 2016b). Therefore, we prefer to suggest that the Gerze dacites may be generated by FC of intermediate magmas compositionally similar to the Bizha diorites. Simple FC modeling shows that fractionating 30% plagioclase of the Bizha dioritic components could produce REE distribution patterns and trace-element trends similar to those of the Gerze dacites (Fig. 6E). The ca. 122 Ma Bizha diorites, located to the east of the Gerze lavas (Fig. 1C), were considered to have been derived from partial melting of a subducted mélange (Hao et al., 2016b). In a subduction channel, sediments, altered oceanic basalts, and hydrated mantle physically mix along the slab-wedge interface to form hybrid mélange rocks (Marschall and Schumacher, 2012; Hao et al., 2016b; Nielsen and Marschall, 2017). The Bizha diorites are slightly older than the Gerze dacites and cannot represent a viable parental magma sensu stricto, yet it is possible that the parental magmas (mélange-derived intermediate melts) with a similar composition to the Bizha diorites could have fractionated to form the Gerze dacites.

Compared to the Gerze dacites, the Gerze andesites show lower SiO_2 and total REE contents and higher MgO contents, indicating possible contribution of mantle components during their generation. Here, we suggest that the involved mantle components could be compositionally similar to the Gerze basalts rather than the Gerze Nb-enriched basalts, because the Gerze Nb-enriched basalts have higher REE and Nb contents than the Gerze andesites. In addition, the Gerze andesites have much more enriched Sr isotopes than the majority of Jurassic–Early Cretaceous crust-derived intermediate-felsic rocks in southern Qiangtang (Y.X. Zhang et al., 2017; Li et al., 2013; Hao et al., 2016a, 2016b), indicating that contamination of such crustal components could not have played a vital role during their generation (Fig. 7A). Rather, the Gerze andesites show enriched Sr-Nd isotopes similar to those of the BangongCo quartz-diorites (Fig. 7A), which originated from a source region involving Amdo basement orthogneisses (Liu et al., 2014). Thus, we infer that the Neoproterozoic–early Paleozoic basement orthogneisses with extremely enriched Sr-Nd isotopes in the Amdo area (Harris et al., 1988) could be an alternative contamination.

Here, simple isotope modeling can be used to illustrate the combined contributions of mantle components and ancient crust in generating the Gerze andesites (Fig. 7B). As the Gerze basalts have no available Sr isotope data due to alteration, the average Sr-Nd isotope values of two Bangong-Nujiang suture zone N-MORBs (with Nd isotopes similar to those of the Gerze basalts) are taken to represent the depleted asthenospheric mantle wedge–derived magmas. The modeling results show that such depleted basaltic magmas contaminated by 15% Amdo basement orthogneisses can yield the Sr-Nd isotopes of the Gerze andesites (Fig. 7B). Therefore, mantle wedge–derived magmas with a similar composition to the Gerze basalts could have been contaminated with ancient Amdo basement to form the Gerze andesites.

Gerze Rhyolites: Jamaican-Type Adakites

The Gerze rhyolites differ from normal arc ADR suites and classic adakites by their higher La/Yb and lower Sr/Y, respectively (Figs. 9C–9D). Interestingly, the distinctive geochemical characteristics of the Gerze rhyolites [high SiO_2 (>70 wt%), low MgO (<2 wt%), high La/Yb, low Sr and Sr/Y (299–343 ppm, <400), and low Y and Yb; Fig. 9] resemble quite closely those of the Newcastle volcanics in Jamaica (Hastie et al., 2010, 2015). Hastie et al. (2010) termed the Newcastle rhyodacites Jamaican-type adakites (JTA), not only to stress their adakitic compositions, but also to highlight the small yet significant geochemical differences between Jamaican-type adakites and "true" adakites. Thus, we suggest that the Gerze rhyolites could be classified as Jamaican-type adakites. Hastie et al. (2010, 2015) suggested that Jamaican-type adakites could only be generated by partial melting of oceanic plateau crust, whereas Shuto et al. (2013) argued that the Ryozen Jamaican-type adakite–like rhyodacites in Japan can be generated by FC processes from a basic magma. We next discuss the petrogenesis and origin of the Gerze Jamaican-type adakites.

The SiO_2-Sr variation diagram (Fig. 9B), which shows slight increases in Sr content with increasing SiO_2, could indicate that plagioclase (Sr-compatible phase) was not fractionated in any significant amount. This is consistent with negligible negative Eu anomalies and positive Sr anomalies of the Gerze Jamaican-type adakites. In addition, substantial garnet and amphibole fractionation of a basic magma can also be precluded, as indicated by the SiO_2-Dy/Yb plot (Fig. 9E). The Philippine adakites were considered to be generated by garnet fractionation from a basic parental magma (Macpherson et al., 2006). However, the Gerze Jamaican-type adakites form a distinct field of SiO_2 versus Dy/Yb and do not have high Dy/Yb ratios relative to the Philippine adakites. Amphibole fractionation of a basaltic magma would form a clearly negative trend in the SiO_2-Dy/Yb plot, as the Lesser Antilles island arc lavas have shown. The Gerze Jamaican-type adakites, with high SiO_2 contents and Dy/Yb ratios, clearly deviate from such a trend. Furthermore, up to 80%–90% FC is required to produce adakitic liquids from a basic magma (e.g., Drummond et al., 1996), corresponding to large cumulates, which are not found in southern Qiangtang. Thus, we argue

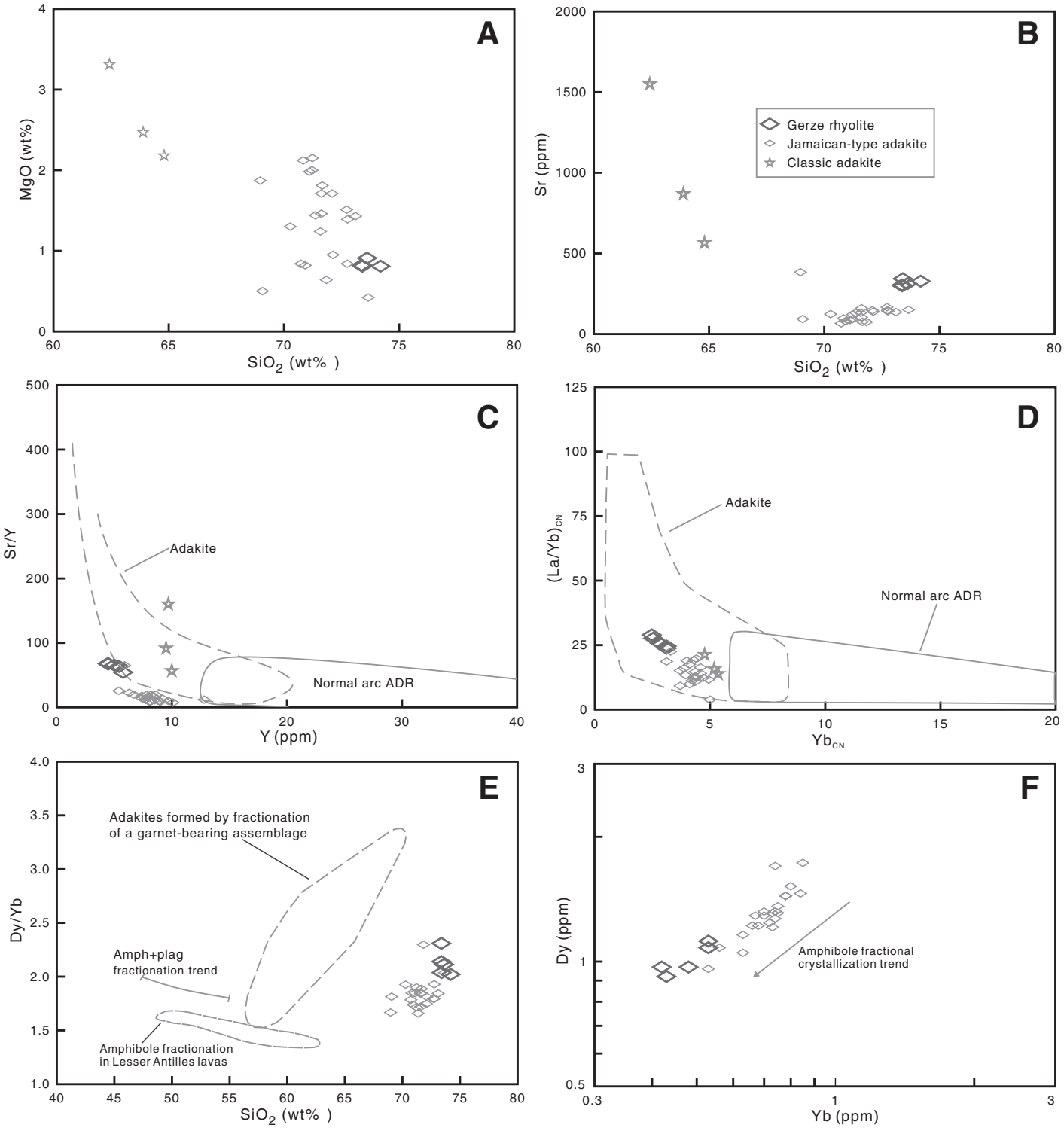

Figure 9. (A) SiO_2 vs. MgO. (B) SiO_2 vs. Sr. (C) Sr/Y vs. Y (Defant and Drummond, 1990). (D) $(La/Yb)_{CN}$ vs. Yb_{CN}, where CN indicates chondrite normalized (Condie, 2005). (E) SiO_2 vs. Dy/Yb (after Hastie et al., 2015). Amph—amphibole; plag—plagioclase. (F) Dy vs. Yb. Jamaican-type adakites (JTA) are from Hastie et al. (2011, 2015). ADR—andesite-dacite-rhyolite.

that the Gerze Jamaican-type adakites could not have been generated by FC of a basic magma, and thus the Jamaican-type adakites data could trace the source region.

The low Sr (<400 ppm) and Al_2O_3 (<19 wt%) contents of the Gerze Jamaican-type adakites should indicate a residual plagioclase in the source region. The significantly fractionated HREEs required a garnet residue. The slightly concave MREE patterns and positive Zr and Hf but negative Ti anomalies can be accounted for by amphibole residue (e.g., Hastie et al., 2010). Thus, the Gerze Jamaican-type adakites were likely derived from a garnet amphibolite source region at relatively low pressures (1.0–1.6 GPa) to stabilize plagioclase.

The differing Nd isotopes of the Gerze Jamaican-type adakites relative to the Bangong-Nujiang suture zone N-MORBs, the Gerze basalts, and the southern Qiangtang continental crust components (Fig. 7A) could imply that they were not derived by partial melting of the metabasic continental crust or a metamorphosed N-MORB oceanic crust. Notably, some Miocene adakites in the Lhasa block, southern Tibet, also show slightly depleted isotopes similar to those of the Gerze Jamaican-type adakites and were suggested to be derived from the relatively juvenile Gangdese arc crust (e.g., L.Y. Zhang et al., 2014). Thus, the possibility that the Gerze rhyolites may be derived from a juvenile crust should be considered. The isotopes of the southern Qiangtang juvenile crust can be represented by those of Early Cretaceous magmatic rocks (Hao et al., 2016b), yet are different from those of the Gerze rhyolites (Fig. 7A). Thus, the juvenile crust should not be taken as the source of the rhyolites. Some normal oceanic slab–derived adakites with isotopes more enriched than N-MORB crust could have a slab origin (basalts and sediments; e.g., the Jurassic adakites in Li et al., 2016). However, the Gerze Jamaican-type adakites could not be derived by such a model. Compared to the Jurassic adakites, more sediment involvement is required to produce the more-enriched isotopes of the Gerze Jamaican-type adakites and will result in higher Th contents and higher Th/Ce ratios, which are not observed in the Gerze Jamaican-type adakites.

In fact, Hastie et al. (2015) conducted numerous partial melting models including different source compositions (MORB, OIB, and oceanic plateau), mineral modes, melt modes, and partition coefficients. The modeling results (see fig. 9 *in* Hastie et al., 2015) clearly illustrate that the Jamaican-type adakites can only be generated by partial melting of plagioclase- and garnet-bearing amphibolite source regions with oceanic plateau–like compositions, rather than with N- and enriched (E) MORBs and OIBs. For instance, fusing an N-MORB, even together with subsequent large degrees of amphibole fractionation, could not produce the high LILE (e.g., Ba and Sr) and LREE (e.g., La) contents of the Jamaican-type adakites. Partial melting of an E-MORB and OIB source, with and without amphibole fractionation, will yield clearly higher La contents and Nb/Yb ratios relative to the Jamaican-type adakites. However, 10% partial melting of an oceanic plateau, together with amphibole fractionation, can well replicate the whole range of the Jamaican-type adakite trace-element data. Indeed, the Dy-Yb variation diagram shows the amphibole FC trend during the formation of the Jamaican-type adakites (Fig. 9F). The Gerze Jamaican-type adakites have extremely similar geochemical features in many aspects, e.g., Nb/Yb ratios, LREE and Sr contents. Therefore, could the Gerze Jamaican-type adakites possibly be generated by fusing an oceanic plateau source?

Recently, most of the ophiolitic fragments across the Bangong-Nujiang suture zone were considered to have been derived dominantly from two oceanic plateaus with age peaks at 185 Ma and 121 Ma, respectively (K.J. Zhang et al., 2014), consistent with distinctly enriched trace-elemental and isotopic compositions of the mafic rocks relative to N-MORB–type oceanic crust (K.J. Zhang et al., 2014; Wang et al., 2016). For example, the Sr-Nd isotopes of these basalts closely resemble those of the Kerguelen Plateau basalts in the Indian Ocean, Tethyan plume-derived basalts, and Ontong Java plateau lavas (see fig. 9 *in* K.J. Zhang et al., 2014). Moreover, shallow-water deposits (e.g., fossil soil horizons, conglomerates, bioclastic limestones) are often present in these Bangong-Nujiang suture zone basalts (e.g., Zhu et al., 2006; K.J. Zhang et al., 2014, 2017), consistent with the abnormal thickness of the basalts (up to 14 km). Combined with the large spatial extent of the Bangong-Nujiang suture zone ophiolitic basalts (from the Rutog to the Amdo, 1000 km long), K.J. Zhang et al. (2014) and Lu et al. (2016) argued that they are likely the remnants of Bangong-Nujiang oceanic plateaus. Here, we adopt such a suggestion. Interestingly, the Sr-Nd isotopic compositions of the Gerze Jamaican-type adakites can be plotted into the field of the Bangong-Nujiang oceanic plateaus (Fig. 7A). Therefore, the Gerze Jamaican-type adakites could be plausibly generated by fusing an oceanic plateau source.

Gerze Nb-Enriched Basalt and Jamaican-Type Adakite Association

The rock association between the Gerze Nb-enriched basalts originating from slab melt–metasomatized mantle wedge and the Gerze Jamaican-type adakites sourced from an oceanic plateau implies a slab-mantle interaction. The Gerze Nb-enriched basalts show isotopic compositions between those of the Gerze Jamaican-type adakites and asthenosphere mantle, suggesting that their mantle source was contaminated with a slab (oceanic plateau) melt.

A slab melt migrating through a mantle wedge will probably react with the mantle peridotites, resulting in the original mineralogy of the peridotite being replaced by precipitating Nb- and Ti-enriched phases (pargasitic amphibole; e.g., Hastie et al., 2011). Such a metasomatized mantle can then be partially melted to generate the high-Nb basalts and Nb-enriched basalts (the Gerze Nb-enriched basalts in this study). Accordingly, the slab melts hybridized by the mantle will lower the SiO_2 contents but elevate the MgO, Ni, and Cr contents (e.g., Hastie et al., 2010). Experiments (Rapp et al., 1999; Rapp and Watson, 1995) show that partial melts of a basaltic source commonly have low MgO (<1.4 wt%), but they will have much higher MgO (>2 wt%) if the resultant liquids were contaminated by mantle peridotites.

The Gerze Jamaican-type adakites have low MgO (<1 wt%), Cr, and Ni contents, and thus the oceanic plateau melts may not have substantially interacted with a peridotite source. This cannot be reconciled with the association between the Gerze Nb-enriched basalts and Jamaican-type adakites. However, similar to the Jamaican-type adakites from Jamaica (Hastie et al., 2015), the Gerze Jamaican-type adakites could have undergone a high degree of amphibole fractionation, effectively obliterating the mantle signature. Mass balance modeling results (Hastie et al., 2015) show that the MgO contents of the parental Jamaican-type adakites magmas could be >3 wt%, consistent with those of melts contaminated by the mantle. For instance, the parental magmas forming the Jamaican-type adakites with 0.8 wt% MgO by fractionating 27%–40% amphibole should have MgO contents of 3.9–5.4 wt%. Thus, partial melts of an oceanic plateau could interact with the mantle and have the expected high MgO, Cr, and Ni contents. The low MgO contents of the Gerze Jamaican-type adakites could be attributed to amphibole fractionation of the hybrid melts. In this way, the Gerze Nb-enriched basalts could have originated from a mantle source metasomatized by the oceanic plateau–derived magmas.

Oceanic Plateau Subduction and Tectonic Evolution of the Bangong-Nujiang Ocean

After contemplating the petrogenesis of the Gerze lavas (basalts, Nb-enriched basaltic

andesites, andesites, dacites, and Jamaica-type adakitic rhyolites), we will now discuss the tectonic evolution of the Bangong-Nujiang Tethyan Ocean.

Closure of the Bangong-Nujiang Ocean

The closure time of the Bangong-Nujiang Ocean remains highly controversial, with two periods hypothesized: the Late Jurassic (e.g., Kapp et al., 2007; Yan et al., 2016; Zhu et al., 2016) and the late Early Cretaceous (e.g., J.X. Li et al., 2014; Fan et al., 2015; K.J. Zhang et al., 2012, 2014; Wang et al., 2016). Here, we identified the Early Cretaceous Gerze lava associations in southern Qiangtang, which provide some constraints on this debate.

Relative to the intermediate-felsic rocks, the mafic rocks are more sensitive to their tectonic settings. The Gerze basalts were sourced from the slab fluid–metasomatized mantle, while the Gerze Nb-enriched basalts originated from a mantle source metasomatized by oceanic plateau–derived magmas. This clearly indicates an oceanic subduction setting, where discrete fluids and melts from the slab arrived at the subarc mantle wedge separately. Similar cases have been observed in the Umnak volcanics, Aleutian arc (Class et al., 2000). Moreover, the source of the Gerze Jamaican-type adakites was a subducted oceanic plateau, and the parental magmas of the Gerze dacites could be the subduction mélange-derived intermediate melts. Therefore, the Gerze lavas were probably generated in a subduction setting. The identification of the subduction-related magmatism in the Gerze area strongly suggests that the northward subduction of the Bangong-Nujiang Ocean continued during the Early Cretaceous. Accordingly, we argue for the closure time of ca. 100 Ma.

Tectonic Evolution of the Bangong-Nujiang Ocean

With the Bangong-Nujiang Ocean closure time of ca. 100 Ma in mind, we suggest that late Mesozoic magmatism (ca. 170–101 Ma) in southern Qiangtang would have been generated in a continental arc setting rather than in a syncollision or postcollisional setting, and therefore it can be attributed to northward oceanic subduction (Zhang et al., 2012). Notably, a striking 20 m.y. magmatic lull (ca. 145–125 Ma) exists in southern Qiangtang (Hao et al., 2016a, 2016b; Liu et al., 2017; J.X. Li et al., 2014; Y.X. Zhang et al., 2017). Any tectonic geodynamics should be well reconciled with such a magmatic gap. Therefore, some geodynamic models (e.g., continuous subduction [J.X. Li et al., 2014], ridge subduction [Xu et al., 2017], and slab break-off [Zhu et al., 2016]) remain questionable because they fail to explain the magmatic gap.

In subduction zones, magmatic lulls have been widely attributed to the disappearance of the asthenospheric wedge (Gutscher et al., 2000) as a result of flat slab subduction. Combined with previous studies (Hao et al., 2016a, 2016b; J.X. Li et al., 2014), we propose a geodynamic model for the Bangong-Nujiang oceanic subduction: normal-angle subduction during 170–145 Ma, flat slab subduction during 145–125 Ma, and subsequent slab roll-back after 125 Ma (Y.X. Zhang et al., 2017). Flat slab subduction is consistent with the N-S crustal shortening of southern Qiangtang since 140–130 Ma (e.g., Kapp et al., 2005, 2007). Similar cases have occurred in the Andes area (e.g., van Hunen et al., 2002). However, the mechanism causing flat slab subduction of the Bangong-Nujiang Ocean remains unknown.

In Central and South American Andes, flat slab subduction was often accompanied by subduction of aseismic ridges or oceanic plateaus, such as the Carnegie Ridge in Ecuador (e.g., Gutscher and Peacock, 2003; Bourdon et al., 2003), the Cocos Ridge in Costa Rica (e.g., Gazel et al., 2015), and the Copiapó Ridge in Chile (e.g., Mulcahy et al., 2014). In fact, when oceanic plateaus or aseismic ridges are subducted (Gerya et al., 2015), the slab angle will gradually become flatter due to their larger buoyancy relative to the normal oceanic crust (Gutscher, 2002), and then flat subduction will occur. A good correlation between flat-slab geometry and aseismic ridge/oceanic plateau subduction has been well demonstrated along the Andes range by geophysical studies (e.g., Nur and Benavraham, 1983; van Hunen et al., 2002).

Therefore, we infer that flat slab subduction of the Bangong-Nujiang Ocean may have been caused by oceanic plateau subduction (Fig. 10). Moreover, the Gerze Jamaican-type adakites and Nb-enriched basalt association, a clear indicator of interactions between subducted oceanic plateau–derived melts and a mantle wedge, could provide supporting evidence for subduction of the Bangong-Nujiang oceanic plateau.

In summary, the tectonic evolution of the Bangong-Nujiang Ocean and associated magmatism in southern Qiangtang can be described as follows (Fig. 10): (1) Jurassic magmatism was generated by normal northward oceanic subduction as suggested in previous studies (e.g., J.X. Li et al., 2014; S.M. Li et al., 2014; Hao et al., 2016a). (2) During 145–125 Ma, subduction of Early Jurassic oceanic plateau beneath southern Qiangtang induced flat slab subduction and the noticeable magmatic gap. Mélange may have formed substantially in a subduction channel during this period, as suggested by Hao et al. (2016b). (3) Subsequent slab roll-back (a transition from flat- to normal-angle subduction) led to asthenospheric convection and renewed magmatism (ca. 125–101 Ma). We infer that the Gerze lavas formed as follows: (1) A combination of fusing of the subducted oceanic plateau, interaction with the mantle wedge, and amphibole FC formed the Gerze Jamaican-type adakitic rhyolites; (2) decompression melting of asthenospheric mantle metasomatized by oceanic plateau–derived melts produced the Gerze Nb-enriched basaltic andesites; (3) fusion of slab fluid–metasomatized

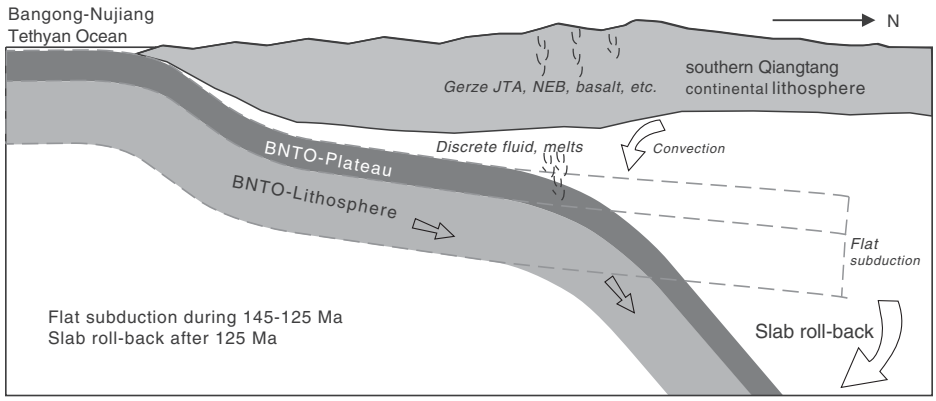

Figure 10. Sketch maps showing the northward subduction geodynamics of the Bangong-Nujiang Ocean (not to scale). Normal subduction during the Jurassic (170–145 Ma) is not shown here, because it has been described in previous studies (e.g., fig. 12 *in* S.M. Li et al., 2014). The dashed lines show flat slab subduction during 145–125 Ma, caused by subduction of the oceanic plateau. After 125 Ma, slab roll-back occurred, inducing asthenosphere convection and magmatic flare-up. The petrogenesis of the Gerze lavas is discussed in more detail in the text. BNTO—Bangong-Nujiang Tethyan Ocean; JTA—Jamaican-type adakites; NEB—Nb-enriched basalts.

asthenospheric mantle yielded the Gerze basalts; (4) which could have been contaminated with ancient Amdo basement to form the Gerze andesites; and (5) the Gerze dacites could have been generated by FC of the subduction mélange–derived intermediate magmas.

CONCLUSIONS

(1) The ca. 110–104 Ma Gerze lavas contain basalts, Nb-enriched basaltic andesites, andesites, dacites, and Jamaica-type adakitic rhyolite. The association between the Gerze Nb-enriched basalt and Jamaican-type adakites implies interactions between the oceanic plateau–derived melts and mantle wedge. The Gerze lavas show clear arc affinities and thus could argue for the closure of the Bangong-Nujiang Ocean at ca. 100 Ma.

(2) Tethyan oceanic plateau subduction during the Early Cretaceous is proposed for the first time to illustrate the tectonic evolution of the Bangong-Nujiang Ocean and distinctive magmatism in southern Qiangtang, central Tibet.

(3) Subduction processes involved in oceanic plateau subduction and roll-back can be effectively revealed by identifying the magmatic gap and subsequent magmatic flare-up and rock associations. This could possibly have important reference implications for other subduction zones.

ACKNOWLEDGMENTS

We are grateful for the constructive comments and suggestions made by Science Editor Brad S. Singer, Associate Editor Wenjiao Xiao, Kai-Jun Zhang, and an anonymous reviewer, which greatly improved the quality of our manuscript. We appreciate the assistance of Y.H. Yang, X.R. Liang, X.L. Tu, J.L. Ma, G.Q. Hu, L.W. Xie, and Y. Liu with zircon age, Lu-Hf isotope, and geochemical analyses. Financial support for this research was provided by the National Key R&D Program of China (no. 2016YFC0600407), the Strategic Priority Research Program (A) of the Chinese Academy of Sciences (no. XDA2007030402), the National Natural Science Foundation of China (no. 41630208 and no. 41573027), the Key Program of the Chinese Academy of Sciences (QYZDJ-SSW-DQC026), Talent Project of Guangdong Province (2014TX01Z079), and Guangzhou Institute of Geochemistry, Chinese Academy of Sciences (GIGCAS) 135 project 135TP201601 and the China Postdoctoral Science Foundation Funded project (grant 2017M620263). This is contribution IS-2573 from GIGCAS. Readers can access our data in the GSA Data Repository (see footnote 1).

REFERENCES CITED

Bao, P., Xiao, X., Su, L., and Wang, J., 2007, Petrological, geochemical and chronological constraints for the tectonic setting of the Dongco ophiolite in Tibet: Science China Earth Sciences, v. 50, p. 660–671, https://doi.org/10.1007/s11430-007-0045-5.

Belousova, E., Griffin, W.L., O'Reilly, S.Y., and Fisher, N., 2002, Igneous zircon: Trace element composition as an indicator of source rock type: Contributions to Mineralogy and Petrology, v. 143, p. 602–622, https://doi.org/10.1007/s00410-002-0364-7.

Bourdon, E., Eissen, J., Gutscher, M.A., Hall, M.L., and Cotten, J., 2003, Magmatic response to early aseismic ridge subduction: The Ecuadorian margin case (South America): Earth and Planetary Science Letters, v. 205, no. 3–4, p. 123–138, https://doi.org/10.1016/S0012-821X(02)01024-5.

Castillo, P.R., Solidum, R.U., and Punongbayan, R.S., 2002, Origin of high field strength element enrichment in the Sulu arc, southern Philippines, revisited: Geology, v. 30, p. 707–710, https://doi.org/10.1130/0091-7613(2002)030<0707:OOHFSE>2.0.CO;2.

Castillo, P.R., Rigby, S.J., and Solidum, R.U., 2007, Origin of high field strength element enrichment in volcanic arcs: Geochemical evidence from the Sulu arc, southern Philippines: Lithos, v. 97, p. 271–288, https://doi.org/10.1016/j.lithos.2006.12.012.

Chang, Q.S., Zhu, D.C., Zhao, Z.D., Dong, G.C., Mo, X.X., Liu, Y.S., and Hu, Z.C., 2011, Zircon U-Pb geochronology and Hf isotopes of the Early Cretaceous Rena Co rhyolites from southern margin of Qiangtang, Tibet, and their implications: Acta Petrolei Sinica, v. 27, p. 2034–2044.

Chen, W.W., Zhang, S.H., Ding, J.K., Zhang, J.H., Zhao, X.X., Zhu, L.D., Yang, W.G., Yang, T.S., Li, H.Y., and Wu, H.C., 2017, Combined paleomagnetic and geochronological study on Cretaceous strata of the Qiangtang terrane, central Tibet: Gondwana Research, v. 41, p. 373–389, https://doi.org/10.1016/j.gr.2015.07.004.

Class, C., Miller, D.M., Goldstein, S.L., and Langmuir, C.H., 2000, Distinguishing melt and fluid subduction components in Umnak volcanics, Aleutian arc: Geochemistry Geophysics Geosystems, v. 1, no. 6, p. 1004–1031, https://doi.org/10.1029/1999GC000010.

Condie, K.C., 2005, TTGs and adakites: Are they both slab melts?: Lithos, v. 80, no. 1–4, p. 33–44, https://doi.org/10.1016/j.lithos.2003.11.001.

Defant, M.J., and Drummond, M.S., 1990, Derivation of some modern arc magmas by melting of young subducted lithosphere: Nature, v. 347, p. 662–665, https://doi.org/10.1038/347662a0.

Drummond, M.S., Defant, M.J., and Kepezhinskas, P.K., 1996, Petrogenesis of slab-derived trondhjemite-tonalite-dacite/adakite magmas: Transactions of the Royal Society of Edinburgh–Earth Sciences, v. 87, p. 205–215, https://doi.org/10.1017/S0263593300006611.

Fan, J.-J., Li, C., Xie, C.-M., Wang, M., and Chen, J.-W., 2015, Petrology and U-Pb zircon geochronology of bimodal volcanic rocks from the Maierze Group, northern Tibet: Constraints on the timing of closure of the Banggong-Nujiang Ocean: Lithos, v. 227, p. 148–160, https://doi.org/10.1016/j.lithos.2015.03.021.

Gazel, E., Hayes, J.L., Hoernle, K., Kelemen, P., Everson, E., Holbrook, W.S., Hauff, F., van den Bogaard, P., Vance, E.A., Chu, S., Calvert, A.J., Carr, M.J., and Yogodzinski, G.M., 2015, Continental crust generated in oceanic arcs: Nature Geoscience, v. 8, p. 321–327, https://doi.org/10.1038/ngeo2392.

Geng, Q., Zhang, Z., Peng, Z., Guan, J., Zhu, X., and Mao, X., 2016, Jurassic–Cretaceous granitoids and related tectono-metallogenesis in the Zapug-Duobuza arc, western Tibet: Ore Geology Reviews, v. 77 p. 163–175, https://doi.org/10.1016/j.oregeorev.2016.02.018.

Gerya, T.V., Stern, R.J., Baes, M., Sobolev, S.V., and Whattam, S.A., 2015, Plate tectonics on the Earth triggered by plume-induced subduction initiation: Nature, v. 527, p. 221–225, https://doi.org/10.1038/nature15752.

Gutscher, M.A., 2002, Andean subduction styles and their effect on thermal structure and intraplate coupling: Earth and Planetary Science Letters, v. 15, p. 3–10.

Gutscher, M.A., and Peacock, S.M., 2003, Thermal models of flat subduction and the rupture zone of great subduction earthquakes: Journal of Geophysical Research, v. 108, no. B1, https://doi.org/10.1029/2001JB000787.

Gutscher, M.A., Eissen, J., and Bourdon, E., 2000, Can slab melting be caused by flat subduction?: Geology, v. 28, no. 6, p. 535–538, https://doi.org/10.1130/0091-7613(2000)28<535:CSMBCB>2.0.CO;2.

Guynn, J., Kapp, P., Pullen, A., Heizler, M., Gehrels, G., and Ding, L., 2006, Tibetan basement rocks near Amdo reveal "missing" Mesozoic tectonism along the Bangong suture, central Tibet: Geology, v. 34, no. 6, p. 505–508, https://doi.org/10.1130/G22453.1.

Hao, L.-L., Wang, Q., Wyman, D.A., Ou, Q., Dan, W., Jiang, Z.-Q., Wu, F.-Y., Yang, J.-H., Long, X.-P., and Li, J., 2016a, Underplating of basaltic magmas and crustal growth in a continental arc: Evidence from late Mesozoic intermediate-felsic intrusive rocks in southern Qiangtang, central Tibet: Lithos, v. 245, p. 223–242, https://doi.org/10.1016/j.lithos.2015.09.015.

Hao, L.-L., Wang, Q., Wyman, D.A., Ou, Q., Dan, W., Jiang, Z.-Q., Yang, J.-H., Li, J., and Long X.-P., 2016b, Andesitic crustal growth via mélange partial melting: Evidence from Early Cretaceous arc dioritic/andesitic rocks in southern Qiangtang, central Tibet: Geochemistry Geophysics Geosystems, v. 17, no. 5, p. 1641–1659, https://doi.org/10.1002/2016GC006248.

Harris, N., Ronghua, X., Lewis, C.L., Hawkesworth, C.J., and Yuquan, Z., 1988, Isotope geochemistry of the 1985 Tibet Geotraverse, Lhasa to Golmud: Philosophical Transactions of the Royal Society, ser. A, v. 327, no. 1594, p. 263–285, https://doi.org/10.1098/rsta.1988.0129.

Hastie, A.R., Kerr, A.C., Pearce, J.A., and Mitchell, S.F., 2007, Classification of altered volcanic island arc rocks using immobile trace elements: Development of the Th-Co discrimination diagram: Journal of Petrology, v. 48, p. 2341–2357, https://doi.org/10.1093/petrology/egm062.

Hastie, A.R., Kerr, A.C., Mcdonald, I., Mitchell, S.F., Pearce, J.A., Wolstencroft, M., and Millar, I.L., 2010, Do Cenozoic analogues support a plate tectonic origin for Earth's earliest continental crust?: Geology, v. 38, no. 6, p. 495–498, https://doi.org/10.1130/G30778.1.

Hastie, A.R., Mitchell, S.F., Kerr, A.C., Minifie, M.J., and Millar, I.L., 2011, Geochemistry of rare high-Nb basalt lavas: Are they derived from a mantle wedge metasomatised by slab melts?: Geochimica et Cosmochimica Acta, v. 75, no. 17, p. 5049–5072, https://doi.org/10.1016/j.gca.2011.06.018.

Hastie, A.R., Fitton, J.G., Mitchell, S.F., Neill, I., Nowell, G.M., and Millar, I.L., 2015, Can fractional crystallization, mixing and assimilation processes be responsible for Jamaican-type adakites? Implications for generating Eoarchaean continental crust: Journal of Petrology, v. 56, p. 1251–1284, https://doi.org/10.1093/petrology/egv029.

Hoskin, P.W., and Schaltegger, U., 2003, The composition of zircon and igneous and metamorphic petrogenesis: Reviews in Mineralogy and Geochemistry, v. 53, no. 1, p. 27–62, https://doi.org/10.2113/0530027.

Huang, T., Xu, J., Chen, J., Wu, J., and Zeng, Y., 2017, Sedimentary record of Jurassic northward subduction of the Bangong-Nujiang Ocean: Insights from detrital zircons: International Geology Review, v. 59, no. 2, p. 166–184, https://doi.org/10.1080/00206814.2016.1218801.

Huang, X.L., Xu, Y.G., Lo, C.H., Wang, R.C., and Lin, C.Y., 2007, Exsolution lamellae in a clinopyroxene megacryst aggregate from Cenozoic basalt, Leizhou Peninsula, South China: Petrography and chemical evolution: Contributions to Mineralogy and Petrology, v. 154, p. 691–705, https://doi.org/10.1007/s00410-007-0218-4.

Kapp, P., Murphy, M.A., Yin, A., Harrison, T.M., Ding, L., and Guo, J.H., 2003, Mesozoic and Cenozoic tectonic evolution of the Shiquanhe area of western Tibet: Tectonics, v. 22, 1029, https://doi.org/10.1029/2001TC001332.

Kapp, P., Yin, A., Harrison, T.M., and Ding, L., 2005, Cretaceous–Tertiary shortening, basin development, and volcanism in central Tibet: Geological Society of America Bulletin, v. 117, p. 865–878, https://doi.org/10.1130/B25595.1.

Kapp, P., Decelles, P.G., Gehrels, G.E., Heizler, M.T., and Ding, L., 2007, Geological records of the Lhasa-Qiangtang and Indo-Asian collisions in the Nima area of central Tibet: Geological Society of America Bulletin, v. 119, no. 7–8, p. 917–933, https://doi.org/10.1130/B26033.1.

Le Bas, M.J., Le Maitre, R.W., Steckeisen, A., and Zanettin, B., 1986, A chemical classification of volcanic rocks based on the total alkali-silica diagram: Journal of Petrology, v. 27, p. 745–750, https://doi.org/10.1093/petrology/27.3.745.

Li, J.X., Qin, K.Z., Li, G.M., Xiao, B., Zhao, J.X., Cao, M.J., and Chen, L., 2013, Petrogenesis of ore-bearing porphyries from the Duolong porphyry Cu-Au deposit, central Tibet: Evidence from U-Pb geochronology, petrochemistry and Sr-Nd-Hf-O isotope characteristics: Lithos, v. 160–161, p. 216–227, https://doi.org/10.1016/j.lithos.2012.12.015.

Li, J.X., Qin, K.Z., Li, G.M., Richards, J.P., Zhao, J.X., and Cao, M.J., 2014, Geochronology, geochemistry, and zircon Hf isotopic compositions of Mesozoic intermediate-felsic intrusions in central Tibet: Petrogenetic and tectonic implications: Lithos, v. 198–199, p. 77–91, https://doi.org/10.1016/j.lithos.2014.03.025.

Li, J.X., Qin, K.Z., Li, G.M., Zhao, J.X., and Cao, M.J., 2015, Petrogenesis of diabase from accretionary prism in the southern Qiangtang terrane, central Tibet: Evidence from U-Pb geochronology, petrochemistry and Sr-Nd-Hf-O isotope characteristics: The Island Arc, v. 24, no. 2, p. 232–244, https://doi.org/10.1111/iar.12107.

Li, Q.L., Li, X.H., Liu, Y., Tang, G.Q., Yang, J.H., and Zhu, W.G., 2010, Precise U-Pb and Pb-Pb dating of Phanerozoic baddeleyite by SIMS with oxygen flooding technique: Journal of Analytical Atomic Spectrometry, v. 25, p. 1107–1113, https://doi.org/10.1039/b923444f.

Li, S., Ding, L., Guilmette, C., Fu, J., Xu, Q., Yue, Y., and Henrique-Pinto, R., 2017, The subduction-accretion history of the Bangong-Nujiang Ocean: Constraints from provenance and geochronology of the Mesozoic strata near Gaize, central Tibet: Tectonophysics, v. 702, p. 42–60, https://doi.org/10.1016/j.tecto.2017.02.023.

Li, S.M., Zhu, D.C., Wang, Q., Zhao, Z.D., Sui, Q.L., Liu, S.A., Liu, D., and Mo, X.X., 2014, Northward subduction of Bangong-Nujiang Tethys: Insight from Late Jurassic intrusive rocks from Bangong Tso in western Tibet: Lithos, v. 205, p. 284–297, https://doi.org/10.1016/j.lithos.2014.07.010.

Li, S.M., Zhu, D.C., Wang, Q., Zhao, Z.D., Zhang, L.L., Liu, S.A., Chang, Q.S., Lu, Y.H., Dai, J.G., and Zheng, Y.C., 2016, Slab-derived adakites and sub-slab asthenosphere-derived OIB-type rocks at 156 ± 2 Ma from the north of Gerze, central Tibet: Records of the Bangong-Nujiang oceanic ridge subduction during the Late Jurassic: Lithos, v. 262, p. 456–469, https://doi.org/10.1016/j.lithos.2016.07.029.

Li, X.H., Li, Z.X., Wingate, M.T.D., Chung, S.L., Liu, Y., Lin, G.C., and Li, W.X., 2006, Geochemistry of the 755 Ma Mundine Well dyke swarm, northwestern Australia: Part of a Neoproterozoic mantle superplume beneath Rodinia?: Precambrian Research, v. 146, p. 1–15, https://doi.org/10.1016/j.precamres.2005.12.007.

Li, X.H., Li, Z., Li, W., Liu, Y., Yuan, C., Wei, G., and Qi, C., 2007, U-Pb zircon, geochemical and Sr-Nd-Hf isotopic constraints on age and origin of Jurassic I- and A-type granites from central Guangdong, SE China: A major igneous event in response to foundering of a subducted flat-slab?: Lithos, v. 96, no. 1–2, p. 186–204, https://doi.org/10.1016/j.lithos.2006.09.018.

Liu, D., Shi, R., Ding, L., Huang, Q., Zhang, X., Yue, Y., and Zhang, L., 2017, Zircon U-Pb age and Hf isotopic compositions of Mesozoic granitoids in southern Qiangtang, Tibet: Implications for the subduction of the Bangong-Nujiang Tethyan Ocean: Gondwana Research, v. 41, p. 157–172, https://doi.org/10.1016/j.gr.2015.04.007.

Liu, D.L., Huang, Q.S., Fan, S.Q., Zhang, L.Y., Shi, R.D., and Ding, L., 2014, Subduction of the Bangong-Nujiang Ocean: Constraints from granites in the Bangong Co area, Tibet: Geological Journal, v. 49, p. 188–206, https://doi.org/10.1002/gj.2510.

Lu, L., Yan, L.L., Li, Q.H., Zeng, L., Jin, X., Zhang, Y.X., Hou, Q.L., and Zhang, K.J., 2016, Oceanic plateau and its significances on the Earth system: A review: Acta Petrologica Sinica, v. 32, no. 6, p. 1851–1876.

Ma, A., Hu, X., Garzanti, E., Han, Z., and Lai, W., 2017, Sedimentary and tectonic evolution of the southern Qiangtang basin: Implications for the Lhasa-Qiangtang collision timing: Journal of Geophysical Research–Solid Earth, v. 122, no. 7, p. 4790–4813, https://doi.org/10.1002/2017JB014211.

Macpherson, C.G., Dreher, S.T., and Thirlwall, M.F., 2006, Adakites without slab melting: High pressure differentiation of island arc magma, Mindanao, the Philippines: Earth and Planetary Science Letters, v. 243, p. 581–593, https://doi.org/10.1016/j.epsl.2005.12.034.

Marschall, H.R., and Schumacher, J.C., 2012, Arc magmas sourced from mélange diapirs in subduction zones: Nature Geoscience, v. 5, p. 862–867, https://doi.org/10.1038/ngeo1634.

Martin, H., Smithies, R.H., Rapp, R.P., Moyen, J., and Champion, D.J., 2005, An overview of adakite, tonalite-trondhjemite-granodiorite (TTG), and sanukitoid: Relationships and some implications for crustal evolution: Lithos, v. 79, no. 1–2, p. 1–24, https://doi.org/10.1016/j.lithos.2004.04.048.

McDonough, W.F., and Sun, S., 1995, The composition of the Earth: Chemical Geology, v. 120, no. 3–4, p. 223–253, https://doi.org/10.1016/0009-2541(94)00140-4.

Mulcahy, P., Chen, C., Kay, S.M., Brown, L.D., Isacks, B.L., Sandvol, E., Heit, B., Yuan, X.H., and Coira, B., 2014, Central Andean mantle and crustal seismicity beneath the Southern Puna plateau and the northern margin of the Chilean-Pampean flat slab: Tectonics, v. 33, no. 8, p. 1636–1658, https://doi.org/10.1002/2013TC003393.

Nielsen, S.G., and Marschall, H.R., 2017, Geochemical evidence for mélange melting in global arcs: Science Advances, v. 3, https://doi.org/10.1126/sciadv.1602402.

Nur, A., and Benavraham, Z., 1983, Volcanic gaps due to oblique consumption of aseismic ridges: Tectonophysics, v. 99, no. 2–4, p. 355–362, https://doi.org/10.1016/0040-1951(83)90112-9.

Otofuji, Y.I., Mu, C.L., Tanaka, K., et al., 2007, Spatial gap between Lhasa and Qiangtang blocks inferred from Middle Jurassic to Cretaceous paleomagnetic data: Earth and Planetary Science Letters, v. 262, p. 581–593, https://doi.org/10.1016/j.epsl.2007.08.013.

Pearce, J.A., 2014, Immobile element fingerprinting of ophiolites: Elements, v. 10, no. 2, p. 101–108, https://doi.org/10.2113/gselements.10.2.101.

Pearce, J.A., and Peate, D., 1995, Tectonic implications of the composition of volcanic arc magmas: Annual Review of Earth and Planetary Sciences, v. 23, p. 251–285, https://doi.org/10.1146/annurev.ea.23.050195.001343.

Peccerillo, R., and Taylor, S.R., 1976, Geochemistry of Eocene calcalkaline volcanic rocks from the Kastamonu area, northern Turkey: Contributions to Mineralogy and Petrology, v. 58, p. 63–81, https://doi.org/10.1007/BF00384745.

Rapp, R.P., and Watson, E.B., 1995, Dehydration melting of metabasalt at 8–32 kbar: Implications for continental growth and crust-mantle recycling: Journal of Petrology, v. 36, p. 891–931, https://doi.org/10.1093/petrology/36.4.891.

Rapp, R.P., Shimizu, N., Norman, M.D., and Applegate, G.S., 1999, Reaction between slab-derived melts and peridotite in the mantle wedge: Experimental constraints at 3.8 GPa: Chemical Geology, v. 160, p. 335–356, https://doi.org/10.1016/S0009-2541(99)00106-0.

Rollinson, H.R., 1993, Using Geochemical Data: Evaluation, Presentation, Interpretation: London, UK, Longman Scientific & Technical, 352 p.

Sajona, F.G., Maury, R.C., Bellon, H., Cotton, J., and Defant, M.J., 1996, High field strength element enrichment of Pliocene–Pleistocene island arc basalts, Zamboanga Peninsula, Western Mindanao (Philippines): Journal of Petrology, v. 37, p. 693–726, https://doi.org/10.1093/petrology/37.3.693.

Shuto, K., Sato, M., Kawabata, H., Osanai, Y., Nakano, N., and Yashima, R., 2013, Petrogenesis of middle Miocene primitive basalt, andesite and garnet-bearing adakitic rhyodacites from the Ryozen Formation: Implications for the tectonomagmatic evolution of the NE Japan Arc: Journal of Petrology, v. 54, p. 2413–2454, https://doi.org/10.1093/petrology/egt052.

Song, P.P., Ding, L., Li, Z.Y., et al., 2017, An early bird from Gondwana: Paleomagnetism of Lower Permian lavas from northern Qiangtang (Tibet) and the geography of the Paleo-Tethys: Earth and Planetary Science Letters, v. 475, p. 119–133, https://doi.org/10.1016/j.epsl.2017.07.023.

Sun, S.S., and McDonough, W.F., 1989, Chemical and isotopic systematics of oceanic basalts: Implications for mantle composition and processes, *in* Saunders, A.D., and Norry, M.J., eds., Magmatism in the Ocean Basins: Geological Society, London, Special Publication 42, p. 313–345, https://doi.org/10.1144/GSL.SP.1989.042.01.19.

Tang, G., Wang, Q., Wyman, D.A., Li, Z., Zhao, Z., Jia, X., and Jiang, Z., 2010, Ridge subduction and crustal growth in the Central Asian orogenic belt: Evidence from late Carboniferous adakites and high-Mg diorites in the western Junggar region, northern Xinjiang (west China): Chemical Geology, v. 277, no. 3–4, p. 281–300, https://doi.org/10.1016/j.chemgeo.2010.08.012.

Tang, G.-J., Cawood, P.A., Wyman, D.A., Wang, Q., and Zhao, Z.-H., 2017, Evolving mantle sources in postcollisional Early Permian–Triassic magmatic rocks in the heart of Tianshan orogen (western China): Geochemistry Geophysics Geosystems, v. 18, p. 4110–4122, https://doi.org/10.1002/2017GC006977.

Tong, Y.B., Yang, Z.Y., Gao, L., Wang, H., Zhang, X.D., An, C.Z., Xu, Y.C., and Han, Z.R., 2015, Paleomagnetism of Upper Cretaceous red-beds from the eastern Qiangtang block: Clockwise rotations and latitudinal translation during the India-Asia collision: Journal of Asian Earth Sciences, v. 114, p. 732–749, https://doi.org/10.1016/j.jseaes.2015.08.016.

van Hunen, J., van den Berg, A.P., and Vlaar, N.J., 2002, The impact of the South-American plate motion and the Nazca Ridge subduction on the flat subduction below south Peru: Geophysical Research Letters, v. 29, no. 14, p. 1690–1724, https://doi.org/10.1029/2001GL014004.

Wang, B.D., Wang, L.Q., Chung, S.L., Chen, J.L., Yin, F.G., Liu, H., Li, X.B., and Chen, L.K., 2016, Evolution of the Bangong-Nujiang Tethyan ocean: Insights from the geochronology and geochemistry of mafic rocks within ophiolite: Lithos, v. 245, p. 18–33, https://doi.org/10.1016/j.lithos.2015.07.016.

Wang, Q., Wyman, A., Xu, J.F., Wan, Y.S., Li, C.F., Zi, F., Jiang, Z.Q., Qiu, H.N., Chu, Z.Y., Zhao, Z.H., and Dong, Y.H., 2008, Triassic Nb-enriched basalts, magnesian andesites, and adakites of the Qiangtang terrane (central Tibet): Evidence for metasomatism by slab-derived melts in the mantle wedge: Contributions to Mineralogy and Petrology, v. 155, p. 473–490, https://doi.org/10.1007/s00410-007-0253-1.

Wu, F.Y., Yang, Y.H., Xie, L.W., Yang, J.H., and Xu, P., 2006, Hf isotopic compositions of the standard zircons and baddeleyites used in U-Pb geochronology: Chemical Geology, v. 234, p. 105–126, https://doi.org/10.1016/j.chemgeo.2006.05.003.

Xie, L.W., Zhang, Y.B., Zhang, H.H., Sun, J.F., and Wu, F.Y., 2008, In situ simultaneous determination of trace elements, U-Pb and Lu-Hf isotopes in zircon and baddeleyite: Chinese Science Bulletin, v. 53, p. 1565–1573.

Xu, W., Li, C., Wang, M., Fan, J.J., Wu, H., and Li, X., 2017, Subduction of a spreading ridge within the Bangong Co–Nujiang Tethys Ocean: Evidence from Early Cretaceous mafic dykes in the Duolong porphyry Cu-Au deposit, western Tibet: Gondwana Research, v. 41, p. 128–141, https://doi.org/10.1016/j.gr.2015.09.010.

Yan, M., Zhang, D., Fang, X., Ren, H., Zhang, W., Zan, J., Song, C., and Zhang, T., 2016, Paleomagnetic data bearing on the Mesozoic deformation of the Qiangtang block: Implications for the evolution of the Paleo- and Meso-Tethys: Gondwana Research, v. 39, p. 292–316, https://doi.org/10.1016/j.gr.2016.01.012.

Yin, A., and Harrison, T.M., 2000, Geologic evolution of the Himalayan-Tibetan orogen: Annual Review of Earth and Planetary Sciences, v. 28, p. 211–280, https://doi.org/10.1146/annurev.earth.28.1.211.

Zhang, K.J., 2004, Secular geochemical variations of the Lower Cretaceous siliciclastic rocks from central Tibet (China) indicate a tectonic transition from continental collision to back-arc rifting: Earth and Planetary Science Letters, v. 229, p. 73–89, https://doi.org/10.1016/j.epsl.2004.10.030.

Zhang, K.J., Xia, B.D., Wang, G.M., Li, Y.T., and Ye, H.F., 2004, Early Cretaceous stratigraphy, depositional environment, sandstone provenance, and tectonic setting of central Tibet, western China: Geological Society of

America Bulletin, v. 116, p. 1202–1222, https://doi.org/10.1130/B25388.1.

Zhang, K.J., Zhang, Y.X., Tang, X.C., Xie, Y.W., Sha, S.L., and Peng, X.J., 2008, First report of eclogites from central Tibet, China: Evidence for ultradeep continental subduction prior to the Cenozoic India-Asian collision: Terra Nova, v. 20, p. 302–308, https://doi.org/10.1111/j.1365-3121.2008.00821.x.

Zhang, K.J., Zhang, Y.X., Tang, X.C., and Xia, B., 2012, Late Mesozoic tectonic evolution and growth of the Tibetan Plateau prior to the Indo-Asian collision: Earth-Science Reviews, v. 114, p. 236–249, https://doi.org/10.1016/j.earscirev.2012.06.001.

Zhang, K.J., Xia, B., Zhang, Y.X., Liu, W.L., Zeng, L., Li, J.F., and Xu, L.F., 2014, Central Tibetan Meso-Tethyan oceanic plateau: Lithos, v. 210–211, p. 278–288, https://doi.org/10.1016/j.lithos.2014.09.004.

Zhang, K.J., Li, Q.H., Yan, L.L., Zeng, L., Lu, L., Zhang, Y.X., Hui, J., Jin, X., and Tang, X.C., 2017, Geochemistry of limestones deposited in various plate tectonic settings: Earth-Science Reviews, v. 167, p. 27–46, https://doi.org/10.1016/j.earscirev.2017.02.003.

Zhang, L.Y., Ducea, M.N., Ding, L., Pullen, A., Kapp, P., and Hoffman, D., 2014, Southern Tibetan Oligocene–Miocene adakites: A record of Indian slab tearing: Lithos, v. 210–211, p. 209–223, https://doi.org/10.1016/j.lithos.2014.09.029.

Zhang, Y.X., Li, Z.W., Yang, W.G., Zhu, L.D., Jin, X., Zhou, X.Y., Tao, G., and Zhang, K.J., 2017, Late Jurassic–Early Cretaceous episodic development of the Bangong Meso-Tethyan subduction: Evidence from elemental and Sr-Nd isotopic geochemistry of arc magmatic rocks, Gaize region, central Tibet, China: Journal of Asian Earth Sciences, v. 135, p. 212–242, https://doi.org/10.1016/j.jseaes.2016.12.043.

Zhu, D.C., Pan, G., Mo, X., Wang, L., Zhao, Z., Liao, Z., Geng, Q., and Dong, G., 2006, Identification for the Mesozoic OIB-type basalts in central Qinghai-Tibetan Plateau: Geochronology, geochemistry and their tectonic setting: Acta Geologica Sinica, v. 80, p. 1312–1328.

Zhu, D.C., Li, S.M., Cawood, P.A., Wang, Q., Zhao, Z.D., Liu, S.A., and Wang, L.Q., 2016, Assembly of the Lhasa and Qiangtang terranes in central Tibet by divergent double subduction: Lithos, v. 245, p. 7–17, https://doi.org/10.1016/j.lithos.2015.06.023.

Science Editor: Bradley S. Singer
Associate Editor: Wenjiao Xiao

Manuscript Received 3 March 2018
Revised Manuscript Received 8 May 2018
Manuscript Accepted 23 August 2018

Printed in the USA